# Normal Faulting Along the Kythira-Antikythira Strait, Southwest Hellenic Forearc, Greece

Violeta Veliz-Borel[1]*, Vasiliki Mouslopoulou[2]*, Andrew Nicol[3], John Begg[4] and Onno Oncken[1]

[1]GFZ Helmholtz Centre Potsdam, German Research Centre for Geosciences, Potsdam, Germany, [2]National Observatory of Athens, Institute of Geodynamics, Athens, Greece, [3]School of Earth and Environment, University of Canterbury, Christchurch, New Zealand, [4]Independent Researcher, Masterton, New Zealand

Upper-plate normal faults along forearcs often accumulate slip during >Mw 6 earthquakes. Such normal faults traverse the forearc of the Hellenic Subduction System (HSS) in Greece and are the focus of this study. Here, we use detailed field-mapping and analysis of high-resolution Digital Elevation Models (DEMs) to study 42 active normal faults on the islands of Kythira and Antikythira in the Aegean Sea. Onshore fault kinematic data are complemented by seabed bathymetry mapping of ten offshore faults that extend along the Kythira-Antikythira Strait (KAS). We find that normal faults in the KAS have lengths of ~1–58 km and scarps ranging in height from 1.5 m to 2.8 km, accommodating, during the Quaternary, trench-orthogonal (NE-SW) extension of ~2.46 ± 1.53 mm/a. Twenty-eight of these faults have ruptured since the Last Glacial Maximum, with their postglacial (16 ± 2 ka) displacement rates (0.19–1.25 mm/a) exceeding their Quaternary (≤0.7–3 Ma) rates (0.03–0.37 mm/a) by more than one order of magnitude. Rate variability, which is more pronounced on short (<8 km) faults, is thought to arise due to temporally clustered paleoearthquakes on individual KAS faults. When displacement accumulation is considered across the entire onshore fault network, rate variability between the two time-intervals examined decreases significantly (2.79 ± 0.41 vs 1.29 ± 0.99 mm/a), a feature that suggests that earthquake clustering in the KAS may occur over ≤16 ka timescales.

Keywords: normal fault, displacement rates, Hellenic Subduction System, forearc, postglacial, earthquake clustering, seismic hazard, Kythira

## 1 INTRODUCTION

Forearc regions along active convergent plate boundaries are broken up by normal and reverse faults which are located at depths of <20 km and are often associated with M < 7 earthquakes (Kelsey et al., 1998; Kato et al., 2011; Mouslopoulou et al., 2014; Robertson et al., 2019; Nicol et al., 2020a). As these upper-plate faults are located above the subducting plate-interface, their activity and kinematics appear to be intimately linked to the mega-thrust seismic cycle (e.g., Mountjoy and Barnes, 2011; Shirzaei et al., 2012; Cortes-Aranda et al., 2015; Menant et al., 2020; Mouslopoulou et al., 2020), while their geometries are largely controlled by the orientation of the subduction trench (Armijo et al., 1992; Moore et al., 2013). Indeed, rupture on upper-plate normal or reverse faults may closely precede (Schurr et al., 2014), follow (Farias et al., 2011; Kato
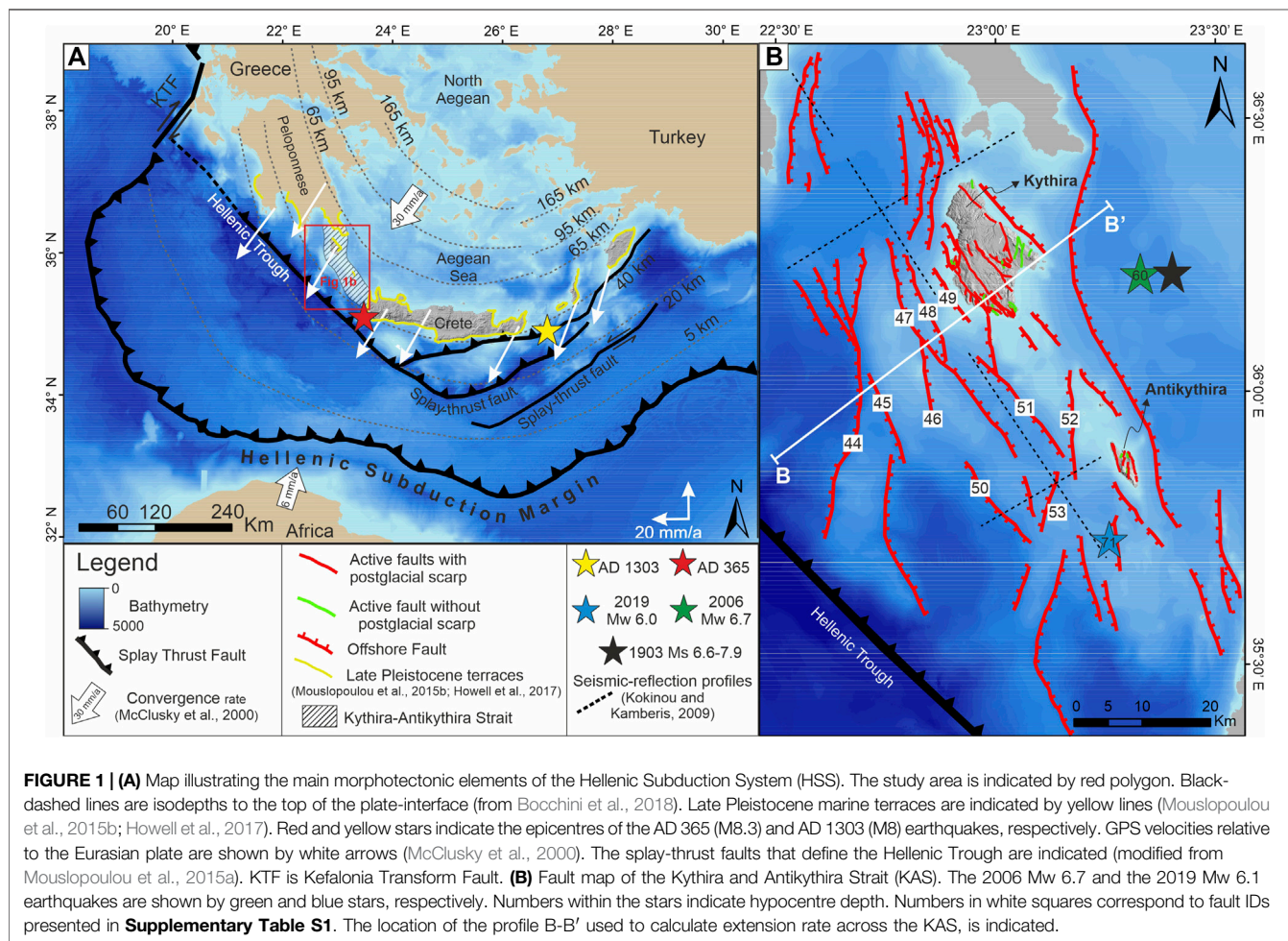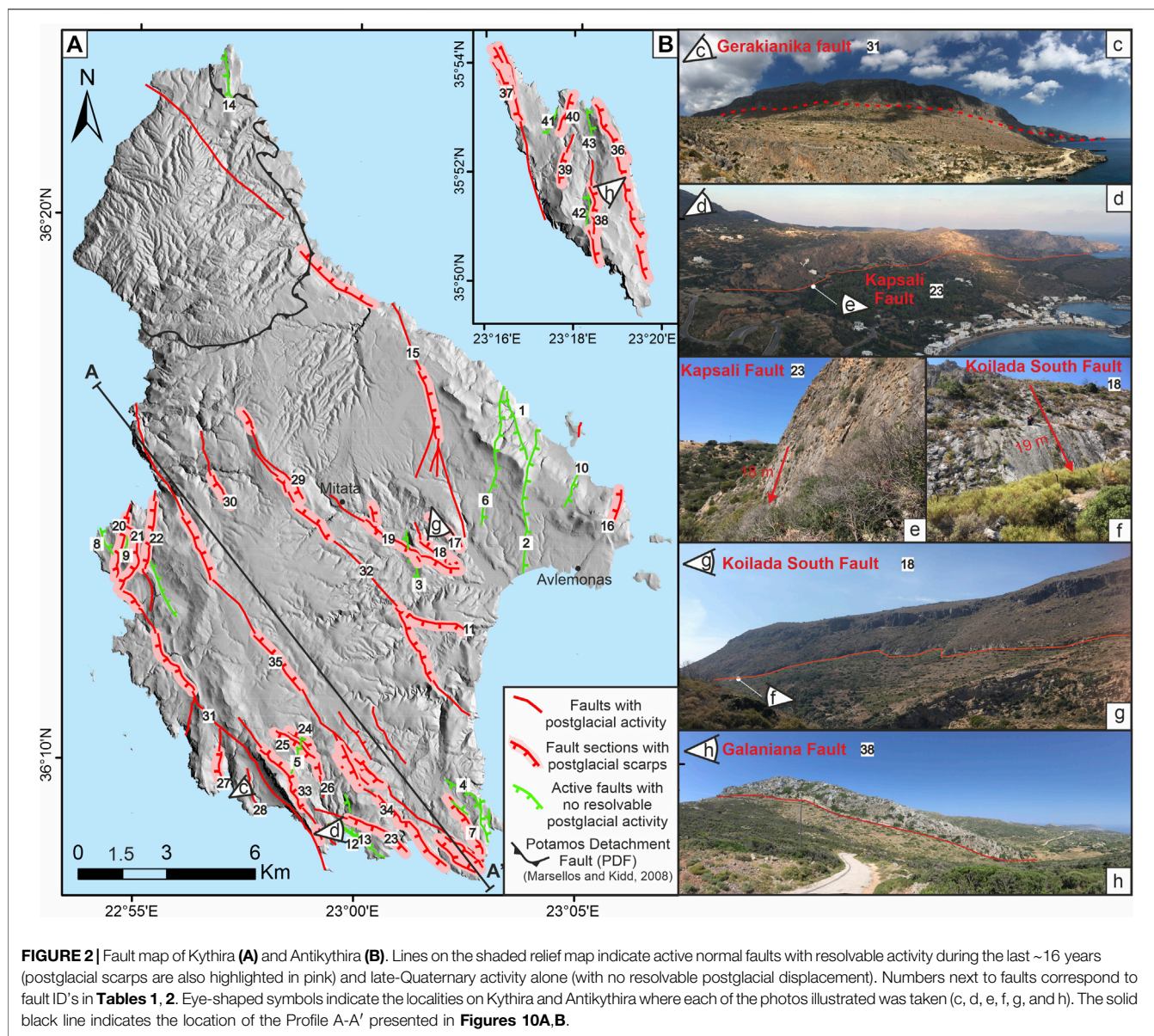
**FIGURE 1 | (A)** Map illustrating the main morphotectonic elements of the Hellenic Subduction System (HSS). The study area is indicated by red polygon. Black-dashed lines are isodepths to the top of the plate-interface (from Bocchini et al., 2018). Late Pleistocene marine terraces are indicated by yellow lines (Mouslopoulou et al., 2015b; Howell et al., 2017). Red and yellow stars indicate the epicentres of the AD 365 (M8.3) and AD 1303 (M8) earthquakes, respectively. GPS velocities relative to the Eurasian plate are shown by white arrows (McClusky et al., 2000). The splay-thrust faults that define the Hellenic Trough are indicated (modified from Mouslopoulou et al., 2015a). KTF is Kefalonia Transform Fault. **(B)** Fault map of the Kythira and Antikythira Strait (KAS). The 2006 Mw 6.7 and the 2019 Mw 6.1 earthquakes are shown by green and blue stars, respectively. Numbers within the stars indicate hypocentre depth. Numbers in white squares correspond to fault IDs presented in **Supplementary Table S1**. The location of the profile B-B′ used to calculate extension rate across the KAS, is indicated.

et al., 2011) or occur in conjunction with megathrust events (Wang et al., 2018; Mouslopoulou et al., 2019). Thus, understanding better this interaction is a pre-requisite to better assessing the kinematics and seismic potential of forearc basins.

The Hellenic Subduction System (HSS) is the fastest converging plate-boundary in the Mediterranean, accommodating ~35–40 mm/a of the relative motion between the African and Eurasian plates (McClusky et al., 2000). Historically, the southern section of the HSS has been the locus of large-magnitude (6<M<8) earthquakes (Papazachos and Papazachou, 1997; Konstantinou, 2010; Andinisari et al., 2020) but also mega-earthquakes (M > 8), such as the AD 365 and the AD 1303 events offshore Crete (Flemming, 1978; Pirazzoli et al., 1982; Ambraseys, 2009) (**Figure 1**). The former events were mostly forearc events produced by extensional faults at shallow depths (<20 km) whereas the latter were mega-thrust earthquakes that ruptured large splay faults within the plate-interface zone (Shaw et al., 2008; Mouslopoulou et al., 2015a, Saltogianni et al., 2020) (**Figure 1**). The upper-plate normal faults studied here are

commonly located in the immediate hanging-wall of these thrust systems (Alves et al., 2007; Shaw and Jackson, 2010; Kokinou et al., 2012; Mouslopoulou et al., 2015a, 2020), forming distinct horst and graben topography in the Hellenic forearc, both onshore (Caputo et al., 2010; Veliz et al., 2018; Nicol et al., 2020a) and offshore (Alves et al., 2007; Sakellariou and Tsampouraki-Kraounaki, 2019). Despite the detailed accounts on the kinematics and seismic potential of the faults within the plate-interface zone (Shaw et al., 2008; Tiberti et al., 2014; Mouslopoulou et al., 2015a; Howell et al., 2017; Saltogianni et al., 2020), to date, little is known about the presence, kinematics and associated seismic hazard of upper-plate normal faulting along the southwest Hellenic forearc (i.e. the islands of Kythira and Antikythira).

Here, we report on the geometries and kinematics of 52 normal faults that traverse the forearc of the southwestern HSS, onshore and offshore the islands of Kythira and Antikythira (**Figures 1**, **2**). We find that at least 26 of these faults that outcrop onshore have ruptured since the Last Glacial Maximum (LGM) (16 ± 2 ka) with average

**FIGURE 2** | Fault map of Kythira **(A)** and Antikythira **(B)**. Lines on the shaded relief map indicate active normal faults with resolvable activity during the last ~16 years (postglacial scarps are also highlighted in pink) and late-Quaternary activity alone (with no resolvable postglacial displacement). Numbers next to faults correspond to fault ID's in **Tables 1**, **2**. Eye-shaped symbols indicate the localities on Kythira and Antikythira where each of the photos illustrated was taken (c, d, e, f, g, and h). The solid black line indicates the location of the Profile A-A′ presented in **Figures 10A,B**.

displacement rates up to 12 times faster than their long-term (≤0.7–3 Ma) rates, especially on short (<8 km) faults. This variability is less pronounced when fault growth is examined over greater spatial scales.

## 1.1 Geological Setting of the Kythira-Antikythira Strait

The Kythira-Antikythira Strait (KAS) extends for about 130 km along the western segment of the HSS, connecting western Crete with southern Peloponnese via a bathymetric ridge (**Figure 1**). The KAS ridge trends ca. N30°W parallel to, and located ca. 50–60 km to the east of, the Hellenic Trough (**Figure 1**). The ridge is 40–50 km wide with an average water-depth of 150–200 m at its crest and is above sea-level on numerous islands, the largest of which are Kythira (maximum altitude

~500 m a.s.l.) and Antikythira (maximum altitude ~370 m a.s.l.). The geometries of Kythira and Antikythira are partly controlled by uplift and subsidence associated with normal faulting (Lyberis et al., 1982; Papanikolaou and Danamos, 1991). Both islands are located on a horst that runs parallel to the ridge and are crossed longitudinally by normal faults, with Kythira (~280 km²) being ~14 times larger than Antikythira (~20 km²). Faulting of these islands is the focus of this study.

The Neogene sedimentary cover in the study area is of Miocene and Pliocene age and rests unconformably on alpine basement rocks of Mesozoic age (limestone, phyllite-quartzite and flysch) (Petrocheilos, 1966; Lyberis et al., 1982; van Hinsbergen et al., 2005). On Kythira, two sedimentary groups are identified: 1) upper-Miocene sedimentary rocks that outcrop near the village of Mitata and are of fluvial, lacustrine and (towards the top) shallow-marine origin; 2) Late-Pliocene

marine sediments (Petrocheilos, 1966). Pliocene sedimentary rocks unconformably overlie the basement and the Miocene deposits (Meulenkamp et al., 1977). The sedimentary cover on the island of Antikythira consists of sandy marls, marly clays and calcarenites as old as of Tortonian age (Lyberis et al., 1982; early Late Miocene).

Van Hinsbergen et al. (2006) reconstructed the vertical movements of the island of Kythira using stratigraphic constraints from Meulenkamp et al. (1977) and found that subsidence followed by rapid uplift occurred over timescales of hundreds of thousands of years. Today, marine terraces are recorded on the islands of Kythira and Antikythira at elevations ranging from 0 to 320 m (**Figure 2**) (Gaki-Papanastassiou et al., 2011), indicating long-term uplift. Although these marine terraces have not been dated, based on stratigraphic relationships they are inferred to be Late Quaternary in age (Gaki-Papanastassiou et al., 2011).

During the Alpine orogeny, the KAS experienced mainly contractional deformation and associated thrust faulting (a process known as nappe stacking; Le Pichon et al., 2002 and references therein). Upper-plate post-Miocene deformation in the KAS is dominated by extension and normal faulting (Lyberis et al., 1982). Normal faults in the KAS have been mapped both onshore (Lyberis et al., 1982; Papanikolaou and Danamos et al., 1991; Doutsos and Kokkalas, 2001; Lekkas et al., 2008; Gaki-Papanastassiou et al., 2011) and offshore (Lyberis et al., 1982; Le Pichon et al., 2002; Kokinou and Kamberis, 2009; Sakellariou and Tsampouraki-Kraounaki, 2019), using a combination of fieldwork, analysis of seismic-reflection lines and bathymetric profiles. Normal faulting on the exhumed Alpine nappe-stack started to dominate, forming a characteristic basin-and-range topography, in the mid-to late-Miocene. Normal faulting was then characterised by a NNW-SSE strike and accommodated extension approximately orthogonal to the trench (Lyberis et al., 1982; Papanikolaou and Danamos, 1991; Marsellos and Kidd, 2008). Post-Miocene ductile and brittle-ductile structures associated with the Potamos Detachment Fault (**Figure 2A**) indicate that significant trench-parallel extension occurred locally in Kythira, possibly during the Pliocene (Papanikolaou and Danamos, 1991; Marsellos and Kidd, 2008). This local change in the kinematics may be associated with the unconformity recorded between the Miocene and Pliocene deposits (Meulenkamp et al., 1977).

The most recent period of deformation commenced in the early Pleistocene (~2.5 Ma) and is, again, associated with extension orthogonal to the trench (Lyberis et al., 1982; Marsellos and Kidd, 2008), which reactivated some of the NW-SE faults. Pleistocene extension and associated normal faulting characterises the entire HSS forearc down to crustal depths of ~20 km and is thought to have produced most of the normal fault displacements recorded in the Hellenic forearc (Angelier et al., 1982; Lyberis et al., 1982; Shaw and Jackson, 2010; Nicol et al., 2020a).

The seismic hazard on the islands of Kythira and Antikythira remained largely unconstrained until the 2006 Mw 6.7 Kythira Earthquake (**Figure 1**). Although that was an intermediate-depth event (60 km) (Konstantinou et al.,

2006) (**Figure 1**), unrelated to the faults studied here, it caused significant damage to buildings and infrastructure at the Kythirian village of Mitata (Lekkas et al., 2008), raising public awareness about the potential seismic hazard in the region. The most well-known examples of historical M > 6 earthquakes in the KAS, include those of 800, 1630, 1750, 1789, 1866, 1889, and 1903 AD (Papadopoulos and Vassilopoulou, 2001 and references therein). From the above list, only the 1866 AD event may be unequivocally characterised as an upper-plate event (Papadopoulos and Vassilopoulou, 2001). The 1889 earthquake may have also been generated in the upper-plate, however, some uncertainty relating to its hypocentral depth remains (Papadopoulos and Vassilopoulou, 2001). The remaining five earthquakes are thought to be deep-sourced events (i.e., either intra-slab or subduction-thrust earthquakes) (Ambraseys et al., 1994; Papazachos and Papazachou, 1997; Papadopoulos and Vassilopoulou, 2001). Besides, no large (M > 6) upper-plate earthquake has occurred within the KAS during the instrumental period (the last approx. 50 years) (https://bbnet.gein.noa.gr/HL/).

## 2 DATA AND METHODS

We have identified and characterised 42 faults that outcrop on the islands of Kythira and Antikythira (**Tables 1**, **2**), together with a further ten offshore faults located within the KAS (**Figure 1**; **Supplementary Table S1**). Onshore fault analysis is based on structural field observations, which were complemented by analysis of a high-resolution DEM (5 m pixel size—data derived from the Greek cadastre agency) from the islands of Kythira and Antikythira using ArcGIS 10.6 (**Figure 2**). Field data include measurements of fault geometries (strike/dip), striations and, scarp heights (vertical fault displacement or throw). Digital mapping of topography on the DEM was used to initially define lineaments which were subsequently ground-truthed during fieldwork. DEMs were also used to estimate fault length and cumulative (long-term) fault displacement, using the topographic changes across fault traces as a first-order proxy for displacement (for details see Nicol et al., 2020a).

The main parameters used to assess fault-slip accumulation through time include fault displacement (D) and fault length (L). Fault displacements were measured in the field using tape-measure (±0.2 m) and on the DEM (±1 m) by collecting topographic profiles along and across faults (**Figure 3**; **Supplementary Figure S1**). Fault displacements were assessed over two distinct time-intervals: 0–16 ± 2 ka and 0–0.7–3 Ma (age constraints are discussed below). As there is no record of creep on normal faults in Greece (Nicol et al., 2020a), while there is plenty of evidence for co-seismic rupture of the ground surface during historic and prehistoric normal fault earthquakes (Papazachos and Papazachou, 1997; Benedetti et al., 2003; Mouslopoulou et al., 2014; Mechernich et al., 2018), the scarps measured here are considered to be the product of repeated large-magnitude (M > 6) earthquakes that have been accrued on faults since the Last Glacial Maximum (LGM), either due to primary or secondary

**TABLE 1 |** Table illustrating the main structural and kinematic characteristics of each fault on the island of Kythira (*error is calculated as +40% and −20% of the total throw measurement; see text for details).

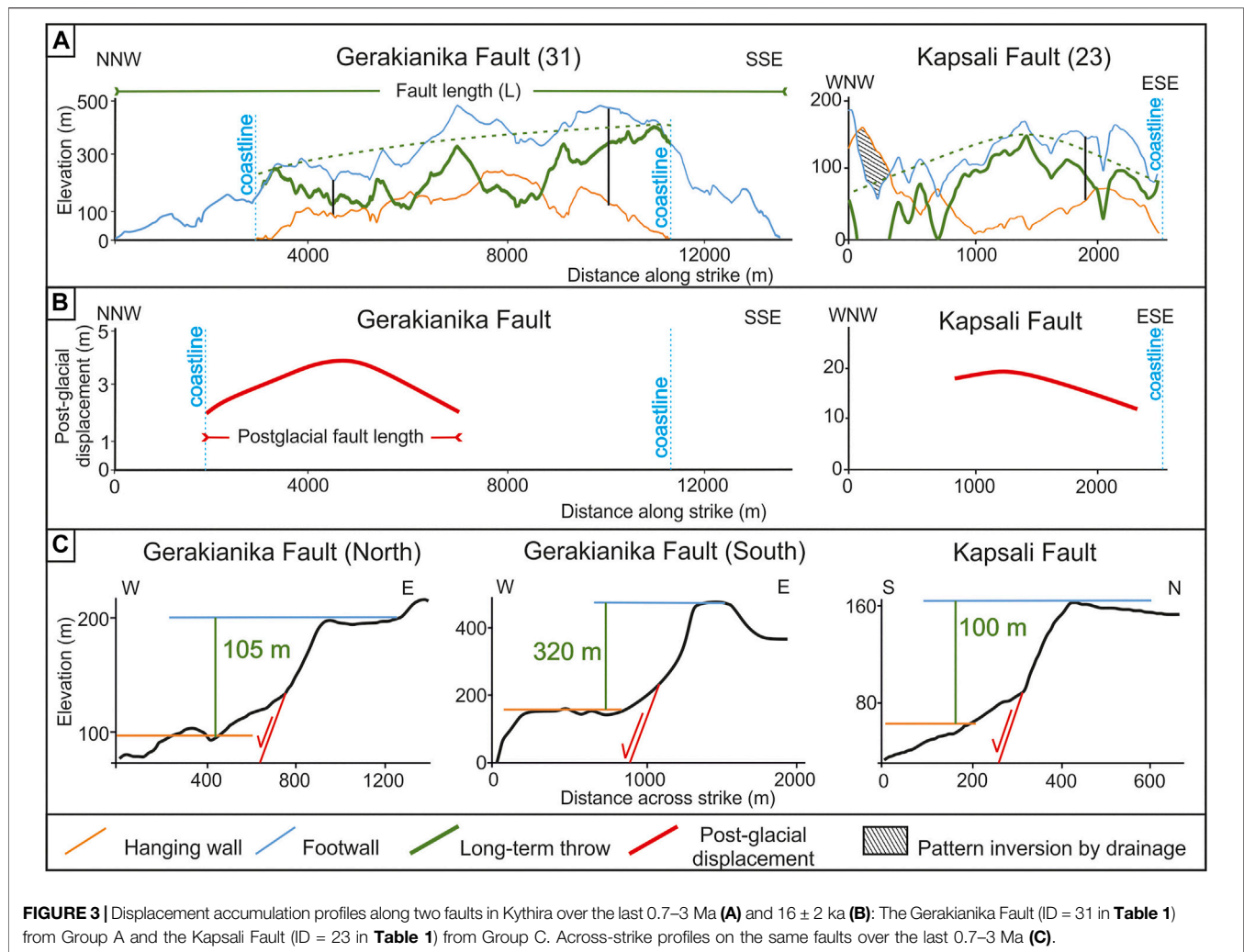| ID | Fault/ Segment Name | Fault group | Av. Strike (°) | Av. Dip (°) | Trend (°) | Plunge (°) | Fault type | Postglacial length (km) | Onshore (*offshore*) topographic length (km) | Postglacial displacement (max) (m) | Error (±) (m) | Displacement rate (16 ± 2 ka) (mm/a) | Error (±) (mm/a) | Quaternary throw (m) (*) | Displacement rate (0.7–3 Ma) (mm/a) | Error* (±) (mm/a) |
|---|---|---|---|---|---|---|---|---|---|---|---|---|---|---|---|---|
| 1 | Joint Moni Fault | B | 168 | 65 | — | — | | — | 2.5 | — | 0 | — | — | 20 | 0.03 | 0.02 |
| 2 | Agia Moni Fault | B | 16 | 84 | — | — | | — | 5 | — | 0 | — | — | 140 | 0.16 | 0.12 |
| 3 | Paleopoli Fault | B | 151 | 66 | 253 | 66 | NR | - | 2.7 | - | 0 | — | — | 90 | 0.11 | 0.09 |
| 5 | Monitochori Fault | B | 10 | 70 | — | — | | — | 1 | — | 0 | — | — | 110 | 0.13 | 0.10 |
| 6 | Kato Moni Fault | B | 355 | 70 | 132 | 62 | NR | — | 5 | — | 0 | — | — | 100 | 0.12 | 0.09 |
| 7 | Kalamos West Fault | B | 179 | 49 | 234 | 43 | NL | 2.7 | 2.7 | 6.7 | 0.5 | 0.42 | 0.10 | 50 | 0.08 | 0.06 |
| 8 | Limnionas 1 Fault | B | — | — | — | — | | — | 1 | — | 0 | — | — | 20 | 0.03 | 0.02 |
| 9 | Limnionas 3 Fault | B | — | — | — | — | | — | 1.7 | — | 0 | — | — | 30 | 0.04 | 0.03 |
| 10 | Diakofti Fault | B | 209 | 72 | — | — | | — | 1.7 | — | 0 | — | — | 15 | 0.02 | 0.01 |
| 14 | Platia Amos Fault | B | 340 | 60 | — | — | | — | 1.8 | — | 0 | — | — | 30 | 0.04 | 0.03 |
| 15 | Aerodromio Fault | B | 355 | 86 | 170 | 52 | NR | 7 | 8 | 6.2 | 0.2 | 0.39 | 0.07 | 80 | 0.09 | 0.07 |
| 16 | Avlemonas Fault | B | 200 | — | — | — | | 1 | 3.3 | 3 | 0.5 | 0.19 | 0.06 | 30 | 0.04 | 0.03 |
| 20 | Limnionas 2 Fault | B | 190 | 70 | — | — | | 1.2 | 2.6 | 5 | 1 | 0.31 | 0.12 | 60 | 0.07 | 0.06 |
| 21 | Limnionas 4 Fault | B | 200 | 60 | — | — | | 2.5 | 2.5 | 4 | 1 | 0.25 | 0.11 | 120 | 0.16 | 0.12 |
| 22 | Kato Chora Fault | B | 183 | 70 | 302 | 67 | NR | 4.2 | 5 | 5 | 1 | 0.31 | 0.12 | 170 | 0.21 | 0.16 |
| 26 | Pano Strapodi Fault | B | 171 | 80 | 261 | 80 | NL | 1 | 1.4 | 8 | 1 | 0.50 | 0.14 | 100 | 0.12 | 0.09 |
| 27 | Melidoni Fault | B | 185 | 60 | 242 | 55 | NL | 1.1 | 2 | 8 | 0.5 | 0.50 | 0.11 | 45 | 0.06 | 0.05 |
| 28 | Felodi Fault | B | 338 | 56 | — | — | | 1.2 | 2 | 1.5 | 0.1 | 0.09 | 0.02 | 20 | 0.03 | 0.02 |
| 4 | Kalamos East Fault | C | 134 | 34 | 184 | 27 | NL | — | 2.8 | — | 0 | — | — | 70 | 0.14 | 0.11 |
| 11 | Alexandrides Fault | C | 100 | — | — | — | | 1 | 3 | 3 | 3 | 0.19 | 0.24 | 140 | 0.18 | 0.13 |

(Continued on following page)

**TABLE 1** | (*Continued*) Table illustrating the main structural and kinematic characteristics of each fault on the island of Kythira (*error is calculated as +40% and −20% of the total throw measurement; see text for details).

| ID | Fault/ Segment Name | Fault group | Av. Strike (°) | Av. Dip (°) | Trend (°) | Plunge (°) | Fault type | Postglacial length (km) | Onshore (*offshore*) topographic length (km) | Postglacial displacement (max) (m) | Error (±) (m) | Displacement rate (16 ± 2 ka) (mm/a) | Error (±) (mm/a) | Quaternary throw (m) (*) | Displacement rate (0.7–3 Ma) (mm/a) | Error* (±) (mm/a) |
|---|---|---|---|---|---|---|---|---|---|---|---|---|---|---|---|---|
| 12 | Chora Fault | C | 310 | 56 | 80 | 49 | NR | — | 2.3 | — | 0 | — | — | 50 | 0.07 | 0.05 |
| 13 | Antichora Fault | C | 135 | 84 | 185 | 82 | NL | — | 1.8 | — | 0 | — | — | 15 | 0.02 | 0.01 |
| 17 | Koiladas North | C | 160 | — | — | — | | 1.3 | 3 | 5 | 0.5 | 0.31 | 0.08 | 60 | 0.08 | 0.06 |
| 18 | Koiladas South | C | 314 | 52 | 20 | 50 | NL | 1.6 | 2.4 | 19 | 1 | 1.19 | 0.24 | 160 | 0.23 | 0.18 |
| 19 | Viaradikas Fault | C | 141 | 59 | 199 | 55 | NL | 4.4 | 5.3 | 8 | 0.5 | 0.50 | 0.11 | 75 | 0.10 | 0.08 |
| 23 | Kapsali Fault | C | 104 | 83 | 256 | 75 | NR | 2.4 | 3 | 18 | 2 | 1.13 | 0.30 | 110 | 0.13 | 0.10 |
| 24 | Klaradika North Fault | C | 310 | 57 | 102 | 36 | NR | 1.1 | 1.1 | 12 | 0.4 | 0.75 | 0.14 | 50 | 0.07 | 0.05 |
| 25 | Klaradika South Fault | C | 107 | 61 | 189 | 61 | NL | 1.6 | 2.6 | 6.5 | 0.2 | 0.41 | 0.07 | 30 | 0.04 | 0.03 |
| 30 | Milopotamos Fault | C | 110 | 54 | 247 | 43 | NR | 1.2 | 2.8 | 3.8 | 0.2 | 0.24 | 0.05 | 80 | 0.11 | 0.09 |
| 31 | Gerakianika fault | A | 158 | 72 | — | — | | 5.5 | 13.8 (*30.5*) | 4 | 0.2 | 0.25 | 0.05 | 320 | 0.38 | 0.29 |
| | Gerakianika north | | 158 | 65 | 243 | 60 | | 5.5 | 7.3 | 4 | 0.2 | 0.25 | 0.05 | 110 | 0.14 | 0.11 |
| | Gerakianika south | | 158 | 78 | 262 | 77 | NL | — | 6.5 | — | 0 | — | — | 320 | 0.37 | 0.28 |
| | Alexandrades -Potamos | A | 330 | 67 | 56 | 50 | NL | 5.6 | 9 | 12 | 1 | 0.75 | 0.18 | 155 | 0.19 | 0.15 |
| 32 | Alexandrades fault | | 330 | 67 | 56 | 50 | NL | 4.6 | 7.3 (*46*) | 12 | 1 | 0.75 | 0.18 | 155 | 0.19 | 0.15 |
| 29 | Potamos Fault | | 164 | 70 | 234 | 69 | NL | 1 | 1.8 | 4.2 | 0.2 | 0.26 | 0.05 | 90 | 0.11 | 0.08 |
| | Drimodas- Strapodi fault | A | — | — | — | — | | 7.3 | 17.5 | 20 | 2.2 | 1.25 | 0.34 | 165 | 0.21 | 0.16 |
| 33 | Strapodi fault | | 141 | 63 | 222 | 43 | NL | 5.6 | 6.8 (*17.5*) | 6 | 0.2 | 0.38 | 0.07 | 55 | 0.07 | 0.05 |
| 34 | Drimodas fault | | 342 | 44 | 76 | 44 | NR | 2.7 | 5.5 | 14 | 2 | 0.88 | 0.27 | 110 | 0.18 | 0.14 |
| 35 | Xeronomiata Fault | A | 325 | 63 | — | — | | 10.2 | 20.5 | 13.3 | 0.8 | 0.83 | 0.18 | 130 | 0.17 | 0.13 |
| | Xeronomiata south | | 313 | 72 | 65 | 71 | NR | 5.4 | 7.2 | 13.3 | 0.8 | 0.83 | 0.18 | 100 | 0.12 | 0.09 |
| | Xeronomiata central | | 330 | 60 | — | — | NR | 1.5 | 6.3 | 3 | 3 | 0.19 | 0.24 | 40 | 0.05 | 0.04 |
| | Xeronomiata North | | 335 | 56 | 86 | 54 | NR | 6.6 | 7 | 8 | 0.5 | 0.50 | 0.11 | 130 | 0.18 | 0.14 |

**TABLE 2 |** Table illustrating the main structural and kinematic characteristics of each fault on the island of Antikythira (*error is calculated as +40% and −20% of the total throw measurement; see text for details).
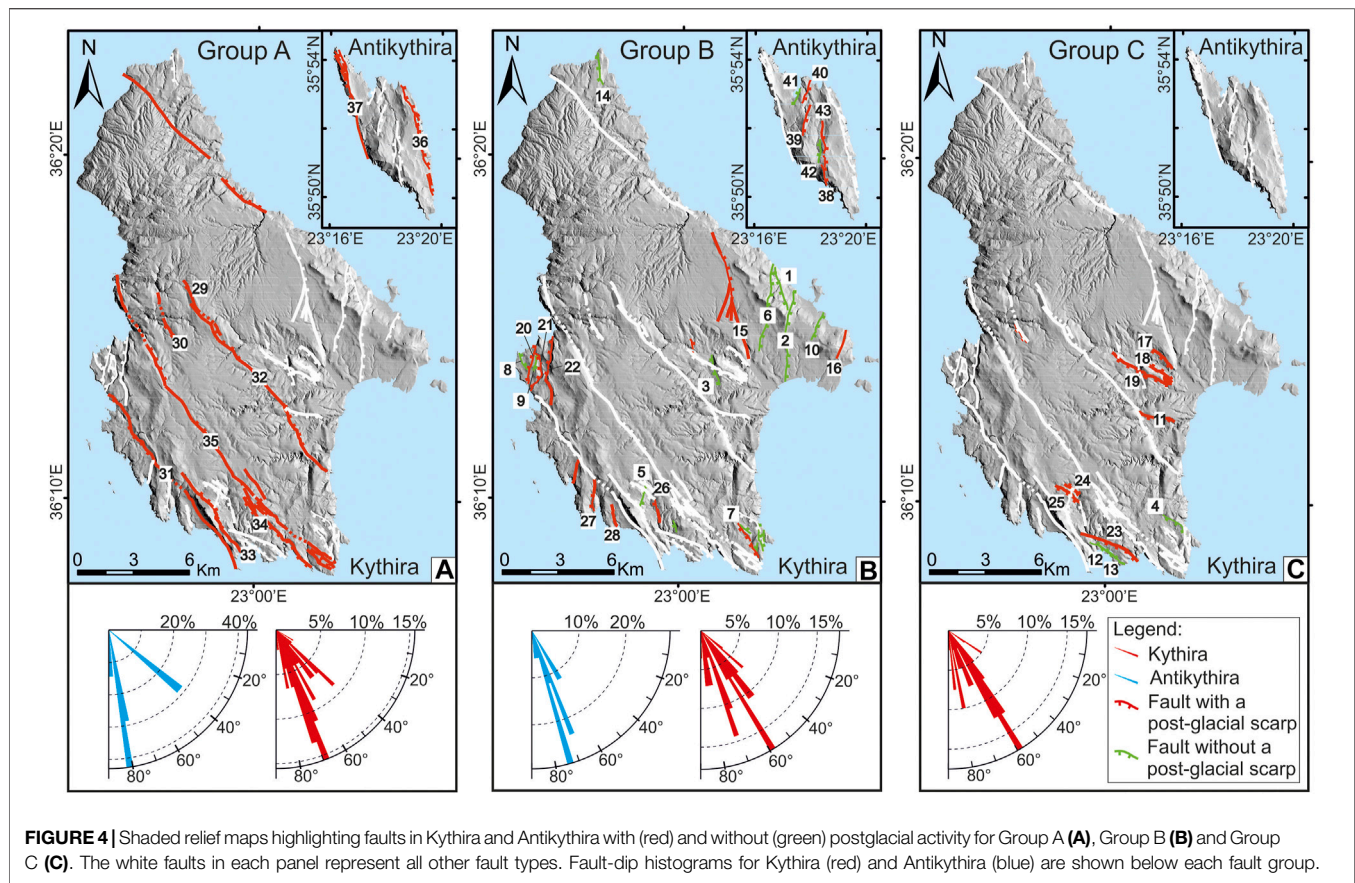
| ID | Fault Name | Fault group | Av. Strike (°) | Av. Dip (°) | Trend (°) | Plunge (°) | Fault type | Postglacial length (km) | Onshore topographic length (km) | Postglacial displacement (max) (m) | Error (±) (m) | Displacement rate (16 ± 2 ka) (mm/a) | Error (±) (mm/a) | Quaternary throw (m) (*) | Displacement rate (0.7–3 Ma) (mm/a) | *Error (±) (mm/a) |
|----|-----------|-------------|----------------|-------------|-----------|------------|------------|------------------------|---------------------------------|-----------------------------------|---------------|--------------------------------------|------------------|--------------------------|-------------------------------------|-------------------|
| 36 | Katsaneviana Fault | A | 18 | 68 | 108 | 86 | NR | 4 | 7 | 6 | 0.5 | 0.38 | 0.08 | 150 | 0.18 | 0.14 |
| 37 | Charchaliana Fault | A | 160 | 60 | — | — | | 6.5 | 6.5 | 9 | 0.2 | 0.57 | 0.08 | 70 | 0.09 | 0.07 |
| 38 | Galaniana Fault | B | 0 | 60 | — | — | | 3 | 3.5 | 7 | 1 | 0.45 | 0.12 | 60 | 0.08 | 0.06 |
| 39 | Pateriana south Fault | B | 20 | 65 | — | — | | 1 | 1.7 | 5 | 0.4 | 0.32 | 0.07 | 40 | 0.05 | 0.04 |
| 40 | Pateriana north Fault | B | 25 | 65 | — | — | | 1 | 1.4 | 8 | 0.4 | 0.51 | 0.09 | 40 | 0.05 | 0.04 |
| 41 | Xiropotamos Fault | B | 220 | 80 | 310 | 80 | NL | 0 | 1 | — | — | — | — | 35 | 0.04 | 0.03 |
| 42 | Antigalaniana Fault | B | 355 | 60 | — | — | | 0 | 1.5 | — | — | — | — | 20 | 0.03 | 0.02 |
| 43 | Xiropotamos East Fault | B | 169 | 75 | 275 | 86 | NR | 0 | 1 | — | — | — | — | 25 | 0.03 | 0.02 |

**FIGURE 3 |** Displacement accumulation profiles along two faults in Kythira over the last 0.7–3 Ma **(A)** and 16 ± 2 ka **(B)**: The Gerakianika Fault (ID = 31 in **Table 1**) from Group A and the Kapsali Fault (ID = 23 in **Table 1**) from Group C. Across-strike profiles on the same faults over the last 0.7–3 Ma **(C)**.

fault-slip. Nevertheless, some creep cannot be completely discounted. The idea of using the carbonate fault scarps in Greece as a measure of postglacial fault activity was first introduced by Benedetti et al. (2002), who dated an active fault scarp near Sparta, using cosmogenic nuclides ($^{36}$Cl). Subsequently, this methodology was applied on numerous other faults in Greece (Benedetti et al., 2003; Mouslopoulou et al., 2014; Mechernich et al., 2018) and eastern Mediterranean (i.e., Benedetti et al., 2013; Tesson et al., 2016; Mozafari et al., 2019; Goodall et al., 2021) to constrain the timing of the exhumation of these scarps. $^{36}$Cl dating from these studies showed that scarp ages consistently ranged between c. 14–20 ka. Here, we adopt the age of 16 ± 2 ka for the onset of normal fault scarp formation, as estimated on the neighbouring island of Crete using $^{36}$Cl dating (Mouslopoulou et al., 2014). This age is within the range of other published $^{36}$Cl ages of fault scarps in Greece (Benedetti et al., 2002, 2003; Mechernich et al., 2018).

Cumulative displacements measured across faults on the two islands postdate the age of the oldest marine sediments, the planation of the islands and, thus, the formation of the oldest (highest) marine terraces. Therefore, the maximum timing of the long-term fault displacements may be indirectly constrained (as no direct age constraints are available) from data presented by Meulenkamp (1985), who identified marine Pliocene deposits (as young as Late Pliocene, ~3 Ma, based on planktic foraminiferal zonation) near the village of Mitata (Kythira) at elevations up to 350 m. This age of marine sediments pre-dates the formation of the highest marine terrace on Kythira. The minimum age for the oldest marine bench can be estimated by direct correlation of marine terraces to Marine Isotopic Stages (MIS). Gaki-Papanasstasiou (2011) traced six terraces below the highest terrace of Kythira (at ~320 masl). In estimating a minimum time interval represented, we interpret that broad and well-developed benches represent sea-level high stands of significant duration, separated by time and uplift from previous high stands. Assuming that the lowest of these marine benches represents MIS 5, counting back, with each preceding odd-numbered MI stage represented by a single high stand, the seventh bench correlates with MIS 17, representing an age of ~700 ka (Lisiecki and Raymo, 2005; Rabineau et al., 2006). At that time (~700 ka), sea-level is estimated at between −10 and −30 m amsl (Rabineau et al., 2006). Therefore, despite the lack of direct age constraints for
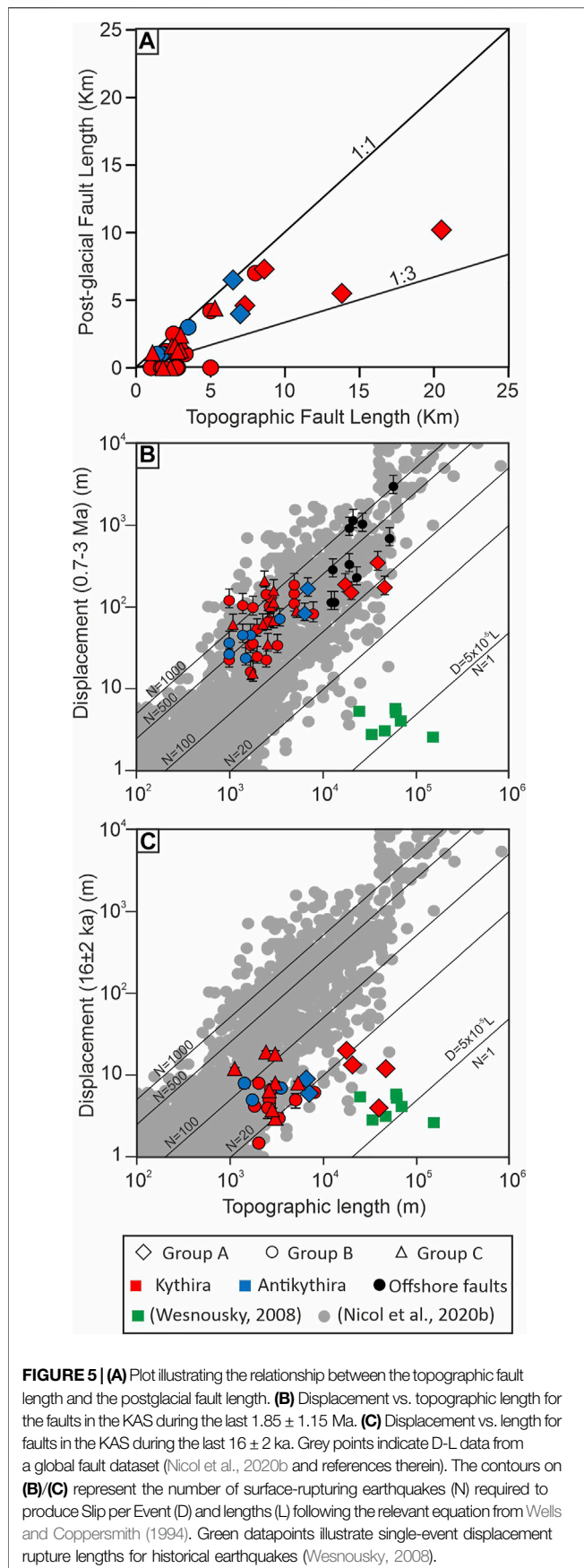
**FIGURE 4** | Shaded relief maps highlighting faults in Kythira and Antikythira with (red) and without (green) postglacial activity for Group A **(A)**, Group B **(B)** and Group C **(C)**. The white faults in each panel represent all other fault types. Fault-dip histograms for Kythira (red) and Antikythira (blue) are shown below each fault group.

the marine benches on the studied islands, indirect age estimates provide first-order observations on the timing of their emergence at 0.7–3 Ma (or 1.85 ± 1.15 Ma).

Post-glacial displacements have been measured for 26 individual faults (~65% of the onshore fault population; see red faults in **Figure 2**). For the remaining onshore faults (n = 16), we measured long-term displacement only, as these faults displayed no postglacial activity (i.e. see green faults in **Figure 2**). Despite the lack of evidence of post ~16 ka displacement on these faults, they are typically associated with steep geomorphic slopes, hanging valleys with reversed drainage and convex across-strike displacement profiles (**Supplementary Figure S1**), features similar to those recorded on faults with proven postglacial activity (e.g. Kapsali and Gerakianika faults in **Figures 3A,C**); when one or more of these features are combined, they are indicative of active normal faulting (Wallace, 1977). The absence of postglacial scarps along some active faults may indicate that they either have not accommodated any surface-rupturing earthquake in the last 16 ± 2 ka, that the scarps produced were rapidly modified by surface processes or that fault throws are too small to be resolved in the DEM (<2 m height). Therefore, all of the mapped fault traces presented in **Figure 2** are inferred to be active (although some have not ruptured during the last ~16 ka).

The discrimination between postglacial from older scarps on the active faults studied is supported by the presence of 'fresh',

polished exhumed planes along the base of older (eroded) scarps. For most faults examined, postglacial scarps were clearly distinguishable from older scarps as they carried striations produced in response to the most recent extension direction (see **Section 3.5**), and were continuous for several hundreds of meters to kilometres (**Figure 2**). To minimise the impact of erosion and deposition that can locally affect the estimates of the postglacial displacements, an effort was made to sample fault scarps along intact fault traces (i.e. where there is no evidence of significant erosion or burial). Scarp height was routinely measured at two to five localities along each fault and preferably near the fault's centre. To minimize uncertainty, between 10 and 20 measurements were collected at each locality (for the range of these values see **Supplementary Table S4**). The postglacial displacements presented for each fault in **Table 1** (Kythira) and **Table 2** (Antikythira) represent the average of the maximum throw recorded in these profiles.

Topographic profiles have been collected along (**Figure 3A** and **Supplementary Figure S1**) and across (**Figure 3C** and **Supplementary Figure S1**) locally over-steepened slopes produced by normal faults. The along-strike profiles represent the hangingwall-footwall separation (i.e. fault throw on each topographic profile was extracted by subtracting the elevation of the hangingwall from the elevation of the footwall). In our effort to minimise uncertainties on the along-strike profiles, we chose a suitable distance from the fault trace (within 250 m from

**FIGURE 5 | (A)** Plot illustrating the relationship between the topographic fault length and the postglacial fault length. **(B)** Displacement vs. topographic length for the faults in the KAS during the last 1.85 ± 1.15 Ma. **(C)** Displacement vs. length for faults in the KAS during the last 16 ± 2 ka. Grey points indicate D-L data from a global fault dataset (Nicol et al., 2020b and references therein). The contours on **(B)/(C)** represent the number of surface-rupturing earthquakes (N) required to produce Slip per Event (D) and lengths (L) following the relevant equation from Wells and Coppersmith (1994). Green datapoints illustrate single-event displacement rupture lengths for historical earthquakes (Wesnousky, 2008).

the fault) to avoid youthful landscape features (i.e. streams, manmade features, etc). In circumstances where a fault involved numerous fault strands/segments, the displacements were aggregated along/across each fault (e.g. the southern tip of Fault 15 in **Figure 2A** or the northern tip of Fault 37 in **Figure 2B**). Maximum fault throw derives from numerous ($n =$ 10) across strike profiles near the fault's centre (e.g. **Figure 3B**). However, the topographic difference between the top and bottom of each range-front should be considered as a minimum, as footwall erosion and hangingwall sedimentation both tend to decrease topography and, hence, could lead to underestimates of the maximum measured long-term throw (Zhang et al., 2017; Nicol et al., 2020a). On the other hand, pre-existing topography could lead to overestimates of fault throw. Here, we are conservative and assign uncertainties of +40% and −20% to maximum fault throws derived from the topography. Post-glacial and cumulative vertical displacements have been subsequently converted into net-displacements on each fault, using the measured fault dips (**Figure 4**).

Offshore faults were derived from analysis of a ~150 m resolution DEM (portal.emodnet-bathymetry.eu/?menu = 19) coupled with published bathymetric maps (Lyberis et al., 1982; Sakellariou and Tsampouraki-Kraounaki, 2019) and seismic-reflection profiles (Kokinou and Kamberis, 2009). As the resolution of the offshore DEM (~150 m) is more than one order of magnitude lower than that onshore (5 m pixel size resolution), here, we were only able to target the larger offshore faults and derive first-order estimates on their throws and geometries to complement the analysis performed onshore. For this reason, our offshore dataset is biased towards the larger faults in the KAS. Bathymetric profiles have been collected across scarps (**Supplementary Figure S2**) recorded on sea-bed and interpreted to result from normal fault-slip at depth. To derive the across-strike profiles for the offshore faults (**Supplementary Figure S2**), the same procedure as for the onshore faults was followed using the bathymetric DEM. The measured cumulative displacements across these faults must postdate initiation of the gently east-dipping East Peloponnese and Kythira detachment systems in the late-Miocene to early Pliocene (Papanikolaou and Royden, 2007). Normal faulting in the KAS is contemporary with development of Pliocene to Quaternary basins east and west of the KAS (Kokinou and Kamberis, 2009; Sakellariou and Tsampouraki-Kraounaki, 2019). Hence, the same age-constraints used for the timing of onshore normal faulting (0.7–3 Ma) is used here to constrain the displacements observed on the sea-floor. Further, we reiterate that the resolution of bathymetric data, coupled with the lack of available subsurface geophysical information that could corroborate our interpretations, may result in uncertainties in the offshore fault length and displacement measurements presented here.

Fault length is an important parameter for estimating earthquake magnitudes and single-event displacement on faults (Wells and Coppersmith, 1994; Wesnousky, 2008). Surface ruptures produced along faults during one or more historic/prehistoric earthquakes often affect only a section of the actual fault length established over thousands to million years

of activity (e.g. topographic fault lengths are greater than the length of historic/prehistoric fault traces; Wesnousky, 2008; Mouslopoulou et al., 2012; Nicol et al., 2016). This may result from a number of reasons, including erosion/burial of small-sized (<2 m) fault scarps, especially along the fault tips where displacements are often small, or earthquakes did not rupture the ground surface along the entirety of the fault (Begg and Mouslopoulou, 2010). The section of faults characterized by postglacial scarp produced during one or more paleoearthquakes is here referred to as the "postglacial length," whereas the section of the fault (with or without a postglacial scarp) associated with a clear topographic signature (with often locally over-steepened slopes and perched valleys) is here referred to as "topographic fault length" (see Nicol et al., 2020a for a detailed discussion). In our calculations of earthquake/fault parameters (**Section 4**), we always use the "topographic length," although to assess the impact of biases in the fault length measurements we have compared "topographic fault lengths" with "postglacial fault lengths" (**Figures 3**, **5A**). In addition, ~60% of the onshore "topographic fault lengths" represent minima as the corresponding faults extend offshore (with three notable exceptions: faults 31, 32, and 34 in **Table 1**, for which the offshore length was traced using bathymetry and seismic-reflection profiles; Kokinou and Kamberis, 2009).

The type of bedrock may also influence the formation and preservation of fault scarps. The faults in the southern section of the island of Kythira traverse mostly limestone, a rock type that enhances scarp preservation, whereas along the northern section of the island the faults, due to the occurrence of the Potamos Detachment (Papanikolaou and Danamos, 1991; Marsellos and Kidd, 2008; **Figure 1**), traverse mainly strongly deformed phyllites-quartzites and flysch (Petrocheilos, 1966), rock types which are both prone to erosion. Thus, fault slip is preferentially preserved at the central-south Kythira with the apparent decrease in the number of active faults in the north of the island possibly relating to rock type (**Figure 2A**). For further discussion on the sampling biases associated with fault and/or earthquake parameters see Nicol et al. (2020a).

## 2.1 Fault Geometries
### 2.1.1 Fault Strike and Dip
Faults have been classified into three groups based on their strike (**Figure 4**). Group A faults have an average strike of N10°W–N30°W, approximately parallel to the average trend of the Hellenic Trench, the Hellenic Trough and the KAS ridge. These are named "Master Faults" here and include four faults on the island of Kythira and two on the island of Antikythira (**Figure 4A**; **Tables 1**, **2**). The Master Faults control the large-scale topography on the islands and have all ruptured during the last 16 ka (**Figure 4A**). Two of these faults on Kythira, the Drimodas and Strapodi faults (faults 33 and 34, respectively, in **Figure 4A**), are analysed jointly as their geometries suggest that they likely merge at depth and are, thus, expected to accrue displacement interdependently (Walsh et al., 2001; Nicol et al., 2006). For the same reasons, displacements have also been aggregated for the Potamos and Alexandrades faults (faults 29 and 32, respectively in **Figure 4A** and **Table 1**). Based on their

strike, the majority of the offshore KAS faults belong also to Group A (**Figure 1** and **Supplementary Table S1**).

The Group B faults strike approximately N-S to N20°E, intersecting the Master faults about 30° clockwise of their trend. On Kythira, these faults are mainly located in the eastern part of the island (**Figure 4B** and **Table 1**). The available bathymetric data do not permit the mapping of the offshore extension of many faults in Group B, although some short-length faults offshore correlate with faults in Group B (e.g., Fault 52 in **Figure 1B**; **Supplementary Table S1**). Onshore Group B faults appear to displace late Pleistocene sediments and marine terraces and about half of them ($n = 9$) have postglacial scarps.

Group C faults strike N60°W (**Figure 4C**), typically terminating against Group A faults. Some of them (e.g. Faults 19 and 3 in **Figure 2A** and **Table 1**) displace faults of Group B to form a structural arrangement that Lyberis et al. (1982) described as "en echelon". The majority of these faults (n = 8, **Supplementary Table S2**) appear to have ruptured during the last ~16 ka, as indicated by their impressive postglacial scarps (up to 19 m; **Figures 2E,F** and **Table 1**). Although the Master Faults (Group A) control the large-scale topography of the islands, it is the small-sized faults (<8 km) of groups B and C that impact the detailed rugosity of the coastline.

Fault dips in the onshore KAS are primarily steep (>60°) (**Figure 4**). Average fault dips measured on exhumed limestone scarps on Kythira range from 60° to 68° (Group A = 64°, Group B = 68°, and Group C = 60°), while on Antikythira these dips range from 64 to 68° (in Groups A and B, respectively; **Figure 4**). Measured onshore dips agree with the average normal fault dips imaged on offshore seismic reflection lines within the western Hellenic forearc (65 ± 5°; Le Pichon et al., 2002; Kokinou and Kamberis, 2009; Mouslopoulou et al., 2020).

### 2.1.2 Fault Lengths
Fault lengths defined by topography (or bathymetry) range in our study area from 1 to 58 km, with faults of Group A generally being longer than those in groups B and C. On the islands of Kythira and Antikythira we have mapped a total of 42 normal faults or fault segments, ranging in length from 1 to 21 km (**Table 1**; **Figures 2A**, **4A–C**). Most of these faults extend offshore, however, their offshore extension could be resolved in only three cases (Faults 31, 32, and 34 in **Figure 2A**) (**Figure 1B** and **Table 1**). Group B onshore fault lengths range from 1 to 8 km while Group C faults have lengths from 1 to 5 km (**Tables 1**, **2**). Offshore fault lengths are constrained by bathymetric data and range from ~10 to 58 km (**Supplementary Table S1**). These faults belong mainly to Group A. The absence of shorter faults offshore (e.g. < 10 km), likely reflects the poorer quality of the bathymetric data compared to the resolution of the DEMs on the islands and for this reason, the offshore dataset should be regarded as incomplete. Nevertheless, analysis of the largest of these faults (**Supplementary Table S1**) contributes to the understanding of fault growth in the KAS.

To assess biases associated with fault-length measurements (see **Section 2**), we compare in the graph of **Figure 5A** the postglacial length of each fault to its corresponding topographic length. We find that postglacial fault lengths are typically up to a

factor of 3 shorter than fault lengths defined by their topographic expressions (**Figure 5A**). This finding is in agreement with many studies of active faults globally that show that trace lengths severely underestimate the total fault length (Wesnousky, 2008; Mouslopoulou et al., 2012; Nicol et al., 2016, 2020a). We follow these studies in suggesting that over multiple seismic cycles the differences between topographic and postglacial fault-trace lengths reflect incompleteness in the sampling of fault-scarps. For this reason, earthquake parameters on individual faults (such as slip per event, earthquake recurrence interval, earthquake magnitude, etc.), are calculated using the topographic fault length.

# 3 RESULTS

## 3.1 Fault Kinematics

Fault horizontal (heave) and vertical (throw) displacements have been determined from postglacial scarps (16 ± 2 ka) and topographic markers (0.7–3 Ma) (see **Section 2** for details). These data have been supplemented by slickenside striations from limestone fault surfaces that define postglacial fault scarps. Fault slip vectors for the last ~16 ka were determined from a total of 115 striations measured on 22 faults (~65% of the total population) in Kythira and 22 striations on three faults (~40% of the total population) in Antikythira (see **Section 3.5**). The sense of fault movement was resolved using displacement of the ground surface and the Petit criteria (Petit, 1987). Striations were mostly recorded at the base of exhumed carbonate scarps (i.e. within <3 m of the ground surface) and near the fault's centre, likely recording movement during their most recent surface-rupturing paleoearthquakes. In general, these striations suggest that onshore faults in the KAS are primarily normal dip-slip with a minor component (<10°) of left-lateral (LN) or right-lateral (RN) strike-slip (**Tables 1, 2**). Of the three groups of faults, Group A, with average strike of N10°W to N30°W, typically accommodates the greatest amount of strike-slip (which is nevertheless negligible).

## 3.2 Long-Term Displacements (0.7–3 Ma)

Long-term displacements provide a measure of fault growth on 100 ka to million-year timescales and of fault finite displacements. The 0.7–3 Ma (long-term) displacements for Group A faults range from 146 to 336 m for Kythira (**Table 1**) and from 81 to 162 m for Antikythira (**Table 2**), while in Group B long-term displacements range from 16 to 181 m for Kythira and from 23 to 69 m for Antikythira. The long-term displacements in Group C faults, which are only present in Kythira (e.g. Kapsali Fault, 23 in **Table 1** and **Figure 2A**), range from 15 to 203 m, while displacements on the offshore faults range from 110 to ~2800 m (**Supplementary Table S1**).

To explore the growth of faults during the last 0.7–3 Ma, we have plotted the long-term displacements for all faults in the KAS as a function of their topographic length (**Figure 5B**). As expected, the graph shows a clear positive relationship between displacement and length, indicating that faults with larger displacements also generally have greater lengths. For
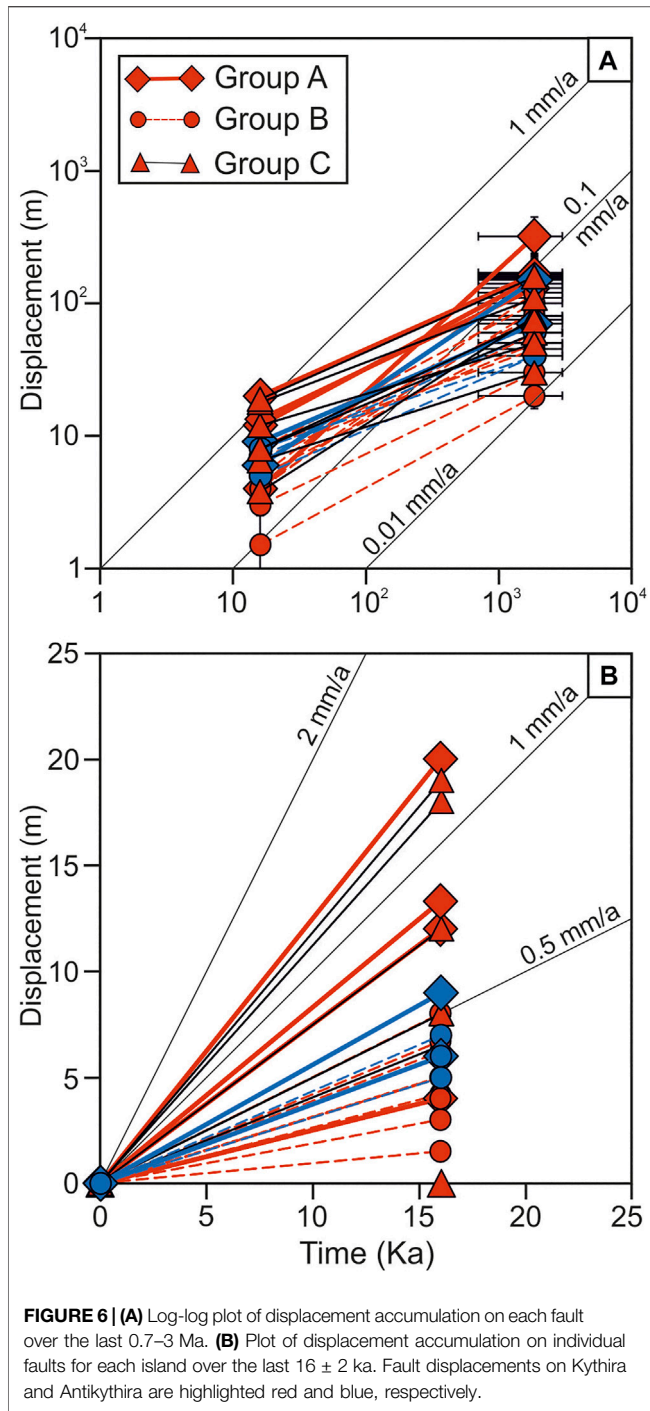
comparison, we have plotted on **Figure 5B** the global dataset for inactive normal faults from Nicol et al. (2020b), and instrumentally recorded historical earthquakes (Wesnousky, 2008). The contours on **Figure 5B** represent the number of surface-rupturing earthquakes (N) required to produce Slip per Event (D) and lengths (L) following the Wells and Coppersmith's (1994) equation $D = 5 \times 10^{-5} L$ for normal faults [e.g. once Slip per Event "D" was calculated, the number 'N' of surface breaking earthquakes was calculated as $N = D/(5 \times 10^{-5} L)$]. We find that the KAS data plot within the field occupied by the global dataset of normal faults with an approximate slope of about 1 (**Figure 5B**). Interestingly, the largest faults in the study area, including those of Group A on the island of Kythira and some of the offshore KAS faults, plot mostly in the lower part of the data field defined by global faults, perhaps indicating that some of these faults are under-displaced (relative to faults sampled globally). Independent of this, the available data support the view that longer faults in the system generally move faster than shorter faults (Nicol et al., 1997).
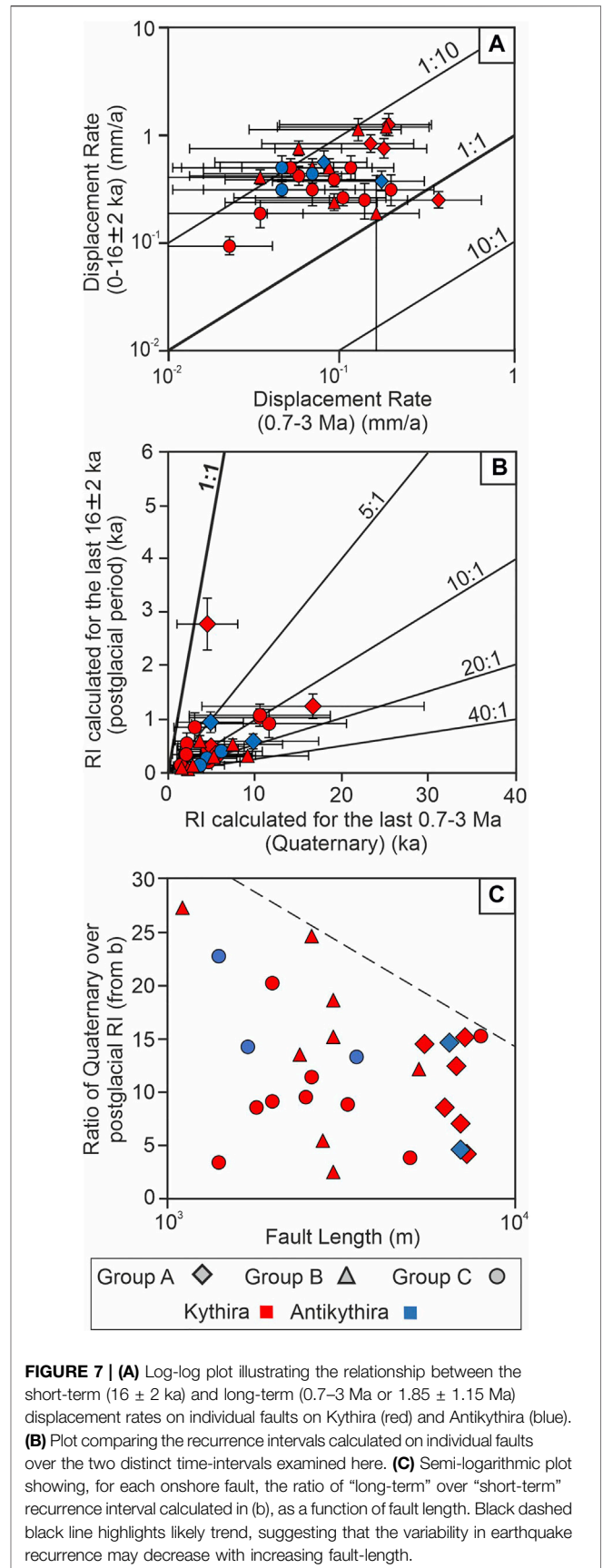
## 3.3 Short-Term Displacement (16 ± 2 ka)

Short-term displacements commonly provide information on slip accumulated during the most recent ground-rupturing earthquakes (Benedetti et al., 2002; Townsend et al., 2010; Mouslopoulou et al., 2014). Here we have measured (in the field) fault displacements for the last ~16 ka (the postglacial time period) (**Figures 2, 3**). All Group A faults in Kythira and Antikythira, together with about 50 and 80% of faults in groups B and C, respectively, have ruptured the ground surface in the last ~16 ka (**Figure 5C**; **Tables 1, 2**). Maximum vertical postglacial displacements on Group A faults range from 4 to 20 m in Kythira (**Table 1**) and from 6 to 9 m in Antikythira (**Table 2**). Faults in Group B have postglacial scarps that range in height on both islands up to 8 m (**Tables 1, 2**), while Group C faults, which were only observed in Kythira, have postglacial scarps up to 19 m in height (**Table 1**).
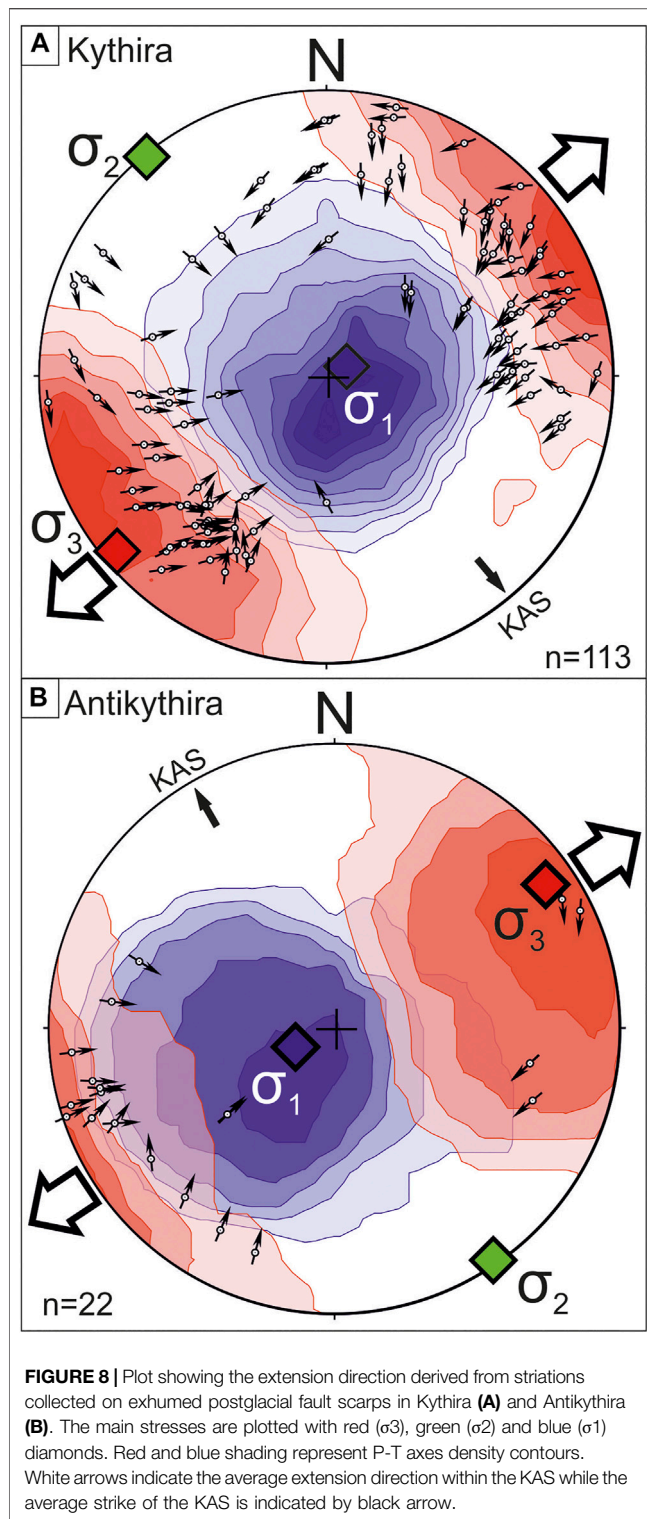
Fault segmentation on individual faults was assessed using the location, strike, dip and along-strike extent of their postglacial scarps. Only the Master Faults (Group A), which are the longest faults on both islands, appear to be segmented (**Figures 2A,B**; **Table 1**). The Gerakianika Fault (Fault 31 in **Figures 2A, 3A,B**), for example, has two segments: the southernmost segment shows no evidence of rupture during the last ~16 ka, while the northernmost segment has a postglacial scarp of up to 4 m height. Similarly, the Xeronomiata Fault has three segments (Fault 35 in **Figure 2A** and **Table 1**): the southernmost segment has a cumulative postglacial throw of ~13 m across four parallel strands; the central segment has no post-glacial scarp, possibly in part due to poor preservation of fault-slip in flysch, while the northernmost segment has a clear continuous postglacial scarp for ~7 km that reaches up to 8 m in height (the largest displacement on a discrete slip surface along the Xeronomiata Fault). In Antikythira, only faults in Group A appear to be segmented (ruptured only partially during the last ~16 ka; **Figure 2B**).

To further explore the postglacial growth of faults on Kythira and Antikythira, we have plotted their postglacial displacements against their topographic length (**Figure 5C**). Unlike the

FIGURE 6 | (A) Log-log plot of displacement accumulation on each fault over the last 0.7–3 Ma. (B) Plot of displacement accumulation on individual faults for each island over the last 16 ± 2 ka. Fault displacements on Kythira and Antikythira are highlighted red and blue, respectively.



FIGURE 7 | (A) Log-log plot illustrating the relationship between the short-term (16 ± 2 ka) and long-term (0.7–3 Ma or 1.85 ± 1.15 Ma) displacement rates on individual faults on Kythira (red) and Antikythira (blue). (B) Plot comparing the recurrence intervals calculated on individual faults over the two distinct time-intervals examined here. (C) Semi-logarithmic plot showing, for each onshore fault, the ratio of "long-term" over "short-term" recurrence interval calculated in (b), as a function of fault length. Black dashed black line highlights likely trend, suggesting that the variability in earthquake recurrence may decrease with increasing fault-length.

positive relationship between D and L for the long-term data, there is no clear relationship for these variables on Kythira and Antikythira over millennial timescales (**Figure 5C**). We also compare here the D-L relationships of the KAS faults with global data for inactive faults (Nicol et al., 2020b) (**Figure 5C**). It is intriguing to observe that, even during this relatively short time-interval (≤16 ± 2 ka), several faults from all groups plot within (although mostly at the lower-end of) the distribution defined by the global D-L dataset (**Figure 5C**). Assuming that the

**FIGURE 8** | Plot showing the extension direction derived from striations collected on exhumed postglacial fault scarps in Kythira **(A)** and Antikythira **(B)**. The main stresses are plotted with red (σ3), green (σ2) and blue (σ1) diamonds. Red and blue shading represent P-T axes density contours. White arrows indicate the average extension direction within the KAS while the average strike of the KAS is indicated by black arrow.

globally (Nicol et al., 2006; Townsend et al., 2010; Benedetti et al., 2013). Fault traces in groups B and C, however, which are all <10 km in length, would require >100 events in the last ~16 ka (**Supplementary Table S3**; **Figure 5C**). This is unrealistic and possibly reveals that (scenario 1) most faults included in Groups B and C are elements (i.e. segments) of larger structures that rupture jointly (**Figure 2**). It may also reflect (scenario 2) triggered secondary fault rupture due to slip on neighbouring faults (e.g. Group A faults). Both of these scenarios are further supported if we consider that most of these small-sized faults in groups B and C are located at the tips of (or proximal to) Group A faults. The implications of multi-fault rupture (scenario 1) and double-counting of paleoearthquakes (scenario 2) to seismic hazard assessment is further discussed in **Section 4**.

## 3.4 Fault Displacement Rates

Displacement rates (DR) were calculated over two distinct time-intervals (0.7–3 Ma and 16 ± 2 ka, using maximum fault displacements accrued over the corresponding time periods (**Figures 6**, **7A**). The Quaternary displacement rates range on Kythira from 0.02 ± 0.01 to 0.38 ± 0.29 mm/a and on Antikythira from 0.03 ± 0.02 to 0.18 ± 0.14 mm/a (**Tables 1**, **2** and **Figure 6A**). The post-glacial (~16 ka) displacement rates range from 0.09 ± 0.02 to 1.25 ± 0.34 mm/a on Kythira, and from 0.32 ± 0.07 to 0.57 ± 0.08 mm/a on Antikythira, with these rates being faster compared to their long-term Quaternary rates, and Group A faults moving on both islands faster than small faults (groups B and C, with faults in group B being the slowest) (**Supplementary Table S2** and **Figures 6A,B**). Nonetheless, **Figure 6B** shows that some faults in Group C, despite their short lengths, have post-glacial rates which are not too dissimilar to those recorded on the Master faults of Group A. Further examination of **Figure 6A** suggests that the majority of the fault growth curves for faults in groups B and C in Kythira and Antikythira are sub-parallel to one another (blue and red dashed lines, respectively, in **Figure 6A**), suggesting uniform growth rates for the same group faults over the last ~0.7–3 Ma. Displacement rates for the offshore faults have been calculated using bathymetric data and an average dip of 65° calculated from offshore seismic studies (Kokinou and Kamberis, 2009). We find that offshore faults have accumulated displacements at rates ranging from 0.13 ± 0.10 to 3.25 ± 2.49 mm/a (**Figure 5B**; **Supplementary Table S1**). The generally faster rates on some of the offshore faults (compared to those onshore) mainly reflect sampling bias towards the longer faults in the system, which are also the faults characterised by greater slip-per-event values. This is because KAS forms a tectonic horst (**Figure 1B**), with the islands of Kythira and Antikythira located at its highest section and large offshore normal faults (several of which were sampled here) forming its flanks.

To explore better the variability in displacement rates on individual faults through time, we have plotted the long-term (0.7–3 Ma or 1.85 ± 1.15 Ma) displacement rate for each KAS fault against its short-term rate (16 ± 2 ka) (**Figure 7A**). These data suggest that, within the uncertainties, most faults in the system appear to have accumulated displacements faster recently

measured slip is primarily seismic, the earthquake contours reveal that, for faults in Group A the observed postglacial scarps require mostly ≤20 paleoearthquakes, consistent with other paleoearthquake datasets from normal faults in Greece (Mouslopoulou et al., 2014; Mechernich et al., 2018) and
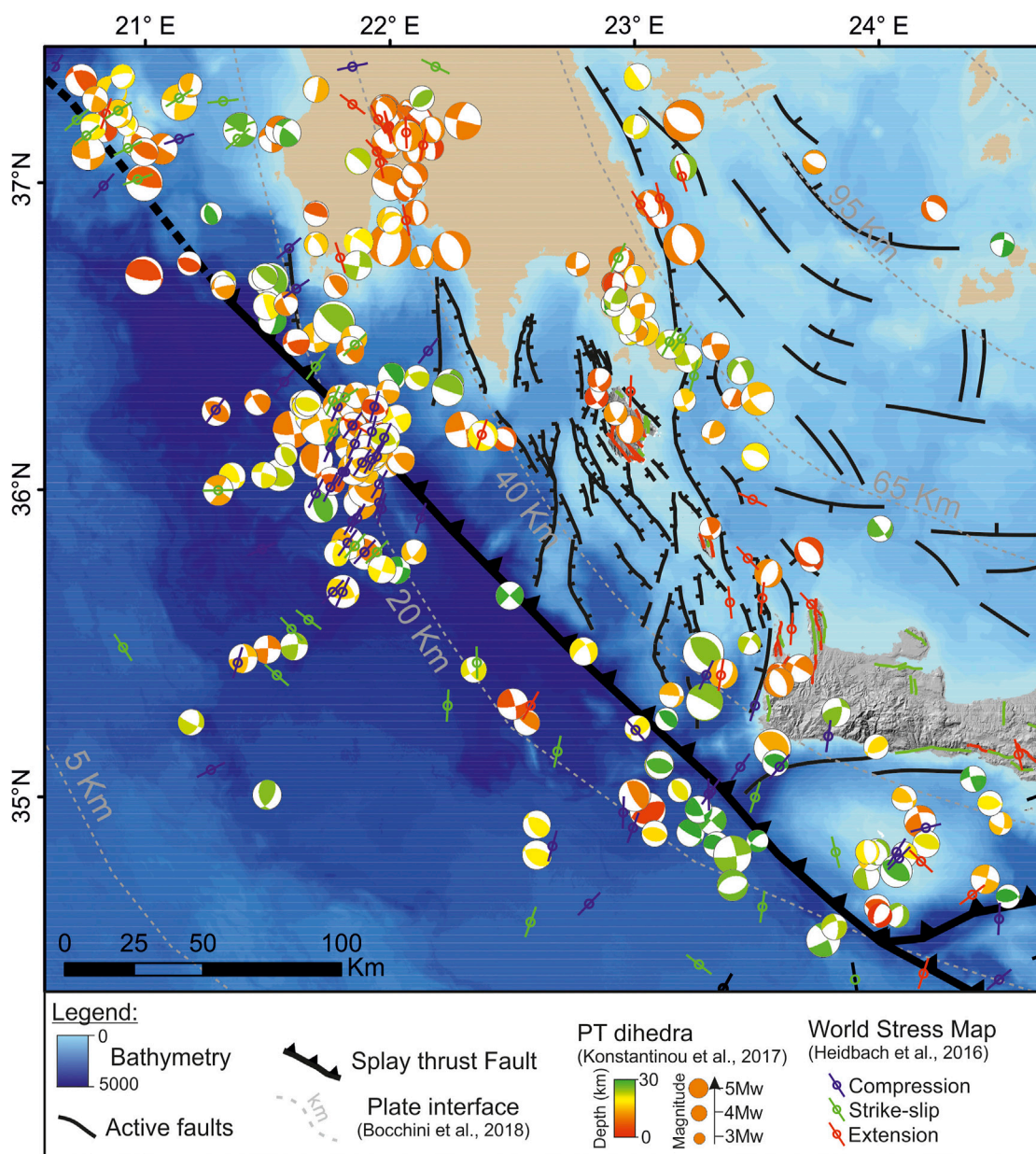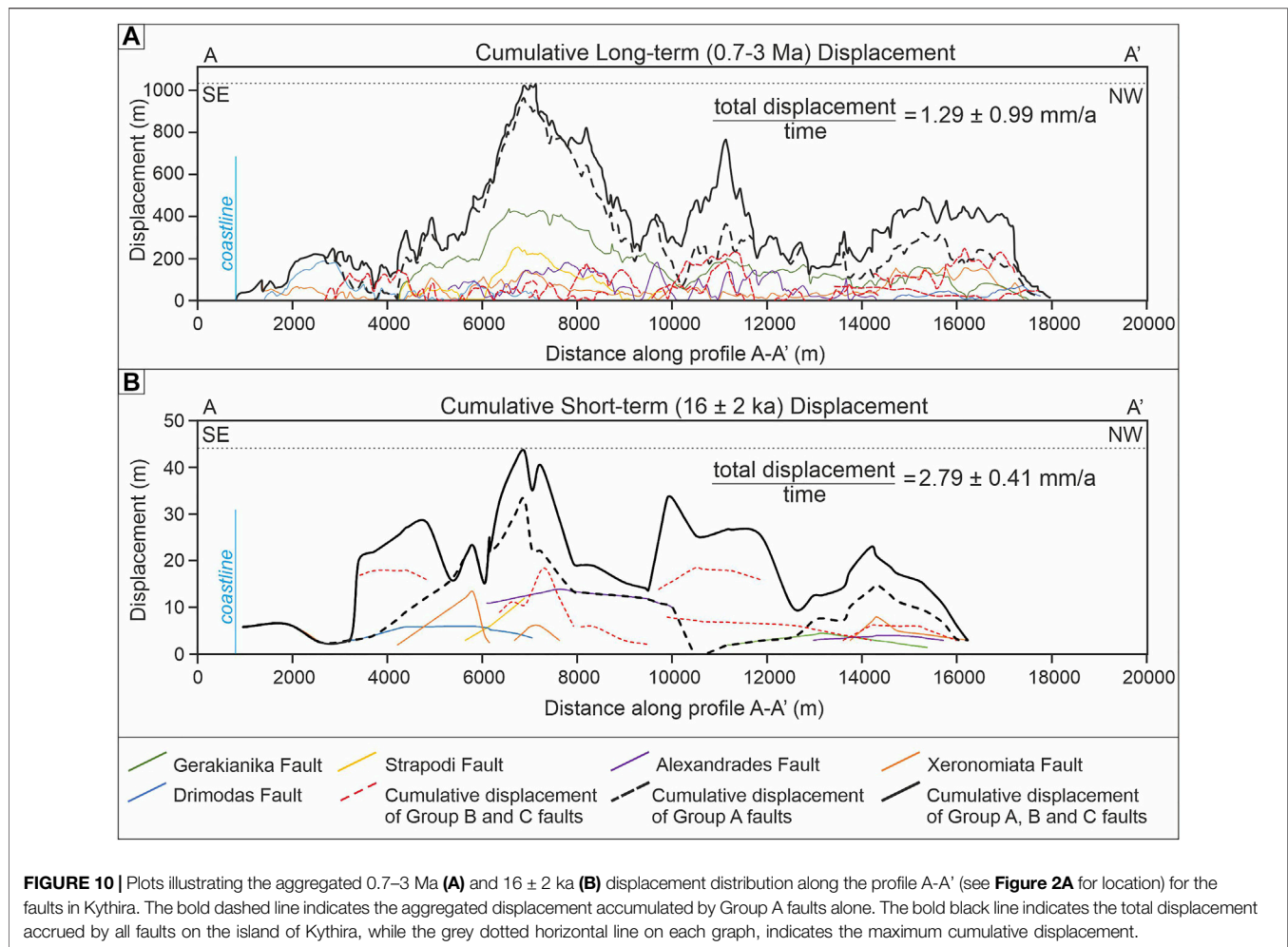
**FIGURE 9 |** Map illustrating the main normal faults along the southwest Hellenic Forearc (this study; Sakellariou and Tsampouraki-Kraounaki, 2019; Nicol et al. 2020a). Moment tensor solutions are from Kontantinou et al. (2017) and are colour-coded according to depth. Present-day stress field indicators are from the World Stress Map Database (Heidbach et al., 2016) and are colour-coded according to stress regime.

(i.e. within the last ~16 ka) compared to the Quaternary, with this variability exceeding one order of magnitude (**Figure 7A**). While the size of this rate variability directly reflects the age uncertainty for the onset of faulting (0.7–3 Ma), even the most conservative scenario (that of faulting initiating at 0.7 Ma) would still produce long-term rates which are, on average, up to seven times lower than their equivalent postglacial rates.

The variability in fault displacement rates (DR) is also reflected in the average earthquake recurrence interval (RI) on these faults (**Figure 7B**), when RI is calculated using both their long-term and short-term displacement rates in conjunction with the calculated slip per event on each fault (RI = $(5 \times 10^{-5} \, {}^*L)/DR$, with L being the topographic fault length for all time periods examined; **Supplementary Table S3**). Data suggest that, with the exception of two faults (ID's 21 and 22) for which the Quaternary earthquake recurrence interval may be shorter than their postglacial recurrence interval (0.6 and 0.7), for all other faults studied the postglacial (16 ± 2 ka) recurrence interval is between ~1.5 and ~50 times shorter compared to their recurrence averaged over the last ~0.7–3 Ma (**Figures 7B,C**

**FIGURE 10 |** Plots illustrating the aggregated 0.7–3 Ma **(A)** and 16 ± 2 ka **(B)** displacement distribution along the profile A-A' (see **Figure 2A** for location) for the faults in Kythira. The bold dashed line indicates the aggregated displacement accumulated by Group A faults alone. The bold black line indicates the total displacement accrued by all faults on the island of Kythira, while the grey dotted horizontal line on each graph, indicates the maximum cumulative displacement.

and **Supplementary Table S3**). The dashed black line in **Figure 7C** reveals that the variability in earthquake recurrence decreases with fault-length (e.g., Nicol et al., 2010), suggesting that for longer faults (>~8 km), the RI's that derive from postglacial displacements may be closer to their average (more representative) values.

## 3.5 Regional Extension Direction and Rates

The extension (strain) and tension (stress) directions for individual faults calculated across the normal fault system (**Figure 8**), provide kinematic and dynamic information about individual earthquakes and regional tectonics. The principal stress axes on both islands were inverted from fault slip using the software SG2PS (Sasvari and Baharev, 2014), with equal weight given to each measurement, while shortening (P) and extensional (T) axes were calculated for each set of striation-fault plane measurements and plotted as contours using the software FaultKin 7.7.4 (**Figure 8**) (Marret and Allmendinger et al., 1990; Allmendinger et al., 2012). Conventionally, slip linear plots are used to reveal subdivision of stress regions by separating crosscutting sets of striations. However, due to the geometric relationships of the studied fault groups (active faults of different

orientations appear to mutually intersect one another), all striations have been here analysed jointly, as local fluctuations in the stress field are expected to arise from fault interactions (see **Section 4**). Still, the results illustrated in **Figure 8** show that on both islands σ1 is sub-vertical, σ2 is sub-horizontal and parallel to both the KAS and the Hellenic Trough, while σ3 is sub-horizontal and perpendicular to the KAS. The σ1 and σ3 plot at the centre of the P-T axes contours (**Figure 8**). Thus, the P–T and stress axes on both islands are broadly consistent with NE-SW extension, in agreement with the geometries of normal-fault moment tensor solutions at < 20 km depth from historic seismicity (**Figure 9**) (Konstantinou et al., 2017).

Although there is some local variability in the orientation of the σ3 and T axes derived from faults across the study area, on a regional scale they both trend NE-SW, approximately orthogonal to the trench and to the strike of the subducting plate (**Figure 9**). The fault and moment tensor data together with the parallelism between the Group A faults and the subduction margin, support the notion that normal faults in the KAS form in response to subduction processes, however, this topic is not addressed here.

To calculate the amount of extension across this section of the Hellenic forearc, we have summed the normal fault displacements

accrued on the largest faults in the onshore and offshore KAS along a margin-perpendicular transect (see Profile B-B′ in **Figure 1B**) and have subsequently converted these displacements into extension rate. The Profile B-B' extends for ~80 km perpendicular to the trench and crosses 14 onshore and offshore KAS faults. The summed throw on these faults is ~6 km (0.8 km for the onshore and 5.2 km for the offshore faults), which produces a long-term fault throw rate of 5.3 ± 3.3 mm/a. Using an average dip of 65° (Kokinou and Kamberis, 2009), we derive a trench-normal extension rate across the KAS of 2.46 ± 1.53 mm/ a. Likely, this is a lower bound as smaller undetected faults and distributed strain are neglected due to resolution limitations in the bathymetric data.

# 4 DISCUSSION

Upper-plate faults that are elements of a single fault system are expected to interact over a range of spatial and temporal scales (i.e. Walsh and Watterson, 1991; Nicol et al., 2006, 2010, 2020b; Dolan et al., 2007). Fault-interactions may be supported by the mostly uniform displacement profiles that arise when the spatial and/or temporal scale of sampling increases to include, respectively, the majority of faults in a system or numerous earthquakes cycles on a fault (Walsh and Watterson, 1991; Nicol et al., 2006, 2010, 2020b; Mouslopoulou et al., 2009; 2012). To assess the degree to which faults in Kythira interact, we have aggregated along the profile A-A' (**Figure 2A**) displacements produced by each fault over the two distinct time-intervals examined (**Figure 10**).

**Figure 10A** illustrates the displacement accumulation on all faults on the island of Kythira during the last ~0.7–3 Ma (long timescales) while **Figure 10B** illustrates the displacement accumulation over the last ~16 ka (short timescales). A first order observation is that displacement accumulation is more variable on shorter than longer timescales on any given fault. Specifically, over short-timescales, displacement accumulation is discontinuous, with some fault sections accommodating large throws while neighbouring segments accruing no displacement (**Figure 10B**). In contrast, throw accumulation on the same faults over long timescales is more uniform, with the wavelength of variability defining distinct fault segments (with individual tips and local maxima; **Figure 10A**). It is interesting to note that, while the Group A faults (e.g., the largest faults in the system) accommodated most displacement over the long-term, it is faults in groups B and C that have produced the greatest displacements during the last ~16 ka (**Figure 10A**) and appear to have higher postglacial than Quaternary rates (**Figure 7A**).

Similar fault behaviour (elevated Holocene rates compared to longer-term rates) has been increasingly observed on many normal fault systems globally (Mouslopoulou et al., 2009, 2012; Nicol et al., 2009), including Greece (Nicol et al., 2020a), where it is ascribed to a combination of earthquake clustering and preferential sampling of those faults that have ruptured recently (Nicol et al., 2009). This phenomenon, which is the earthquake equivalent of the "Sadler Effect" (Sadler, 1981) reported for sedimentary systems, likely conceals from our fault record a

significant number of active faults due to resolution/ preservation issues for which the postglacial rates will be lower than their Quaternary rates. The comparison of rates on individual faults that derive from different timescales, also suggests that rate variability decreases with increasing fault length (**Figure 7A**). This feature likely suggests that for the longer faults (>~8 km) in the system, the time-window of ~16 ka approaches (or, in some cases, exceeds) the duration of earthquake clustering.

While displacement accumulation along individual faults is to a lesser or greater extent variable on both timescales, the aggregated (across all faults) displacement profile along A-A' appears to reproduce a large semi-triangular profile, centred at ~7 km (black lines in **Figures 10A,B**, respectively), that may typify normal faults (Manzocchi et al., 2006). Despite the incompleteness of the dataset, this finding suggests that faults on the island of Kythira interact to produce coherent growth patterns over spatial scales of ~20 km and over temporal scales of ≥16 ka. The approximately uniform fault growth over greater length (temporal and/or spatial) scales is reflected in the comparable, within the uncertainties, displacement rates on Kythira through time (1.29 ± 0.99 mm/a over ~0.7–3 Ma and to 2.79 ± 0.41 mm/a over ~16 ka) (**Figure 10**). This, in turn, suggests that while large-magnitude earthquake clustering on individual faults span timescales >16 ka, when most faults in the system are considered, clustering of large-magnitude earthquakes within the system occurs over timescales ≤16 ka. Both short-term earthquake clustering on individual faults (e.g. **Figure 7B**) and system-wide stability in displacement accumulation (e.g. **Figures 6A**, **10A**) are features that characterise normal fault systems and require fault interactions (Nicol et al., 2006; 2010). Fault interactions have been independently confirmed by multi-fault ruptures during large-magnitude earthquakes in various geotectonic settings, such as the M6.4 1987 Edgecumbe and M7.8 2016 Kaikoura earthquakes in New Zealand, the M6.6–6.7 1981 Alkyonides Earthquake Sequence in Greece, the ~M8 Lisbon earthquake, etc (Jackson et al., 1982; Vilanova et al., 2003; Wesnousky, 2008; Begg and Mouslopoulou, 2010; Mouslopoulou et al., 2019).

To assess the seismic hazard associated with rupture of faults in the KAS we have calculated the maximum earthquake magnitude using the empirical equation of Wells and Coppersmith (1994), assuming negligible creep (Mw = 4.86 + 1.32*log(L); **Supplementary Table S3**). Analysis shows that the faults in the KAS that belong to groups B and C are not capable of producing ground-rupturing earthquakes alone, as the maximum earthquake magnitudes range from M < 5 to M 5.9. In contrast, all six faults of Group A may produce ground-rupturing earthquakes, the magnitude of which may range from M6 to M6.9 (**Supplementary Table S3**). When scenarios of combined rupture are considered (Group A faults together with faults from groups B or C), earthquakes of up to M7 may be achieved. But as the total length of most faults in the KAS remains unconstrained, these magnitudes should be considered as minima.

Considering only the faults of Group A, ~85 large-magnitude (M > 6) paleoearthquakes may have ruptured

the ground surface in the onshore KAS during the last ~16 ka (**Supplementary Table S3**). Although this would require one event in the KAS every about ~190 years (**Supplementary Table S3**), which contradicts the historic record (that suggests one or two events in the last 1000 years; see **Section 1.1**), many of these events are expected to occur in clusters. It is also possible that the estimated number (~85) of large-magnitude earthquakes in the KAS overestimates the actual number of events that ruptured the ground surface because some paleoearthquakes may have produced slip on more than one faults of Group A, leading to double counting of events. Uncertainties in the onshore fault length, from which the number of paleoearthquakes is indirectly calculated, may have also contributed to this mismatch. Post-glacial slip on the remaining faults (groups B and C) is thought to have resulted either from their combined rupture with faults from Group A or as secondary slip due to primary rupture on the neighbouring faults of Group A. In any case, the role of multi-fault ruptures during Aegean earthquakes and their impact on seismic hazard assessment warrants further investigation.

# 5 CONCLUSION

Normal faulting in the KAS accommodates extension approximately orthogonal to the trench in the brittle upper crust of the Hellenic forearc and is associated with a wide range of fault lengths and displacements. Upper-plate faulting is here examined over two distinct time intervals (0.7–3 Ma and 16 ± 2 ka). We find that, over million-year timescales, large faults (Group A) accumulate larger displacements and move faster than small faults (Group B & C faults). However, over millennial timescales (~0–16 ka), large and small faults in the KAS accumulate displacements in a highly variable manner. Analysis shows that small faults (<8 km) have, on average, up to 12 times faster displacement rates (compared to their long-term rates) although only ~80% of these faults have ruptured in the postglacial times. We also find that when the spatial scale of observation is increased to sample most faults in the KAS,

displacement rate variability decreases significantly, possibly due to fault interactions. The latter is found to have significant impact on the calculation of seismic parameters, especially on small faults.

# DATA AVAILABILITY STATEMENT

The original contributions presented in the study are included in the article/**Supplementary Material**, further inquiries can be directed to the corresponding authors.

# AUTHOR CONTRIBUTIONS

VV-B and VM designed the project. VV-B, JB and VM performed the fieldwork while VV-B analysed all data and wrote the first draft (under the supervision of VM). All authors discussed the results, provided feedback and commented on the manuscript.

# ACKNOWLEDGMENTS

# SUPPLEMENTARY MATERIAL

The Supplementary Material for this article can be found online at: https://www.frontiersin.org/articles/10.3389/feart.2021.730806/full#supplementary-material

# REFERENCES

Allmendinger, R. W., Cardozo, N. C., and Fisher, D. (2012). *Structural Geology Algorithms: Vectors & Tensors*. Cambridge: Cambridge University Press.

Alves, T. M., Lykousis, V., Sakellariou, D., Alexandri, S., and Nomikou, P. (2007). Constraining the Origin and Evolution of Confined Turbidite Systems: Southern Cretan Margin, Eastern Mediterranean Sea (34°30-36°N). *Geo-mar Lett.* 27, 41–61. doi:10.1007/s00367-006-0051-1

Ambraseys, N. (2009). *Earthquakes in the Mediterranean and Middle East: A Multidisciplinary Study of Seismicity up to 1900*. Cambridge: Cambridge University Press. doi:10.1017/CBO9781139195430

Ambraseys, N. N., Melville, C. P., and Adams, R. D. (1994). *The Seismicity of Egypt, Arabia and the Red Sea: A Historical Review*. Cambridge: Cambridge Univ. Press. doi:10.1017/CBO9780511524912

Andinisari, R., Konstantinou, K. I., and Ranjan, P. (2020). Seismotectonics of SE Aegean Inferred from Precise Relative Locations of Shallow Crustal Earthquakes. *J. Seismol.* 24, 1–22. doi:10.1007/s10950-019-09881-8

Angelier, J., Lybéris, N., Le Pichon, X., Barrier, E., and Huchon, P. (1982). The Tectonic Development of the Hellenic Arc and the Sea of Crete: a Synthesis. *Tectonophysics* 86, 159–196. doi:10.1016/0040-1951(82)90066-X

Armijo, R., Lyon-Caen, H., and Papanastassiou, D. (1992). East-west Extension and Holocene normal-fault Scarps in the Hellenic Arc. *Geol* 20, 491–494. doi:10.1130/0091-7613(1992)020<0491:eweahn>2.3.co;2

Begg, J. G., and Mouslopoulou, V. (2010). Analysis of Late Holocene Faulting within an Active Rift Using Lidar, Taupo Rift, New Zealand. *J. Volcanology Geothermal Res.* 190, 152–167. doi:10.1016/j.jvolgeores.2009.06.001

Benedetti, L., Finkel, R., King, G., Armijo, R., Papanastassiou, D., Ryerson, F. J., et al. (2003). Motion on the Kaparelli Fault (Greece) Prior to the 1981 Earthquake Sequence Determined from 36Cl Cosmogenic Dating. *Terra Nova* 15, 118–124. doi:10.1046/j.1365-3121.2003.00474.x

Benedetti, L., Finkel, R., Papanastassiou, D., King, G., Armijo, R., Ryerson, F., et al. (2002). Post-glacial Slip History of the Sparta Fault (Greece) Determined by36Cl Cosmogenic Dating: Evidence for Non-periodic Earthquakes. *Geophys. Res. Lett.* 29, 87-1–87-4. doi:10.1029/2001GL014510

Benedetti, L., Manighetti, I., Gaudemer, Y., Finkel, R., Malavieille, J., Pou, K., et al. (2013). Earthquake Synchrony and Clustering on Fucino Faults (Central Italy) as Revealed from *In Situ*36Cl Exposure Dating. *J. Geophys. Res. Solid Earth* 118, 4948–4974. doi:10.1002/jgrb.50299

Bocchini, G. M., Brüstle, A., Becker, D., Meier, T., van Keken, P. E., Ruscic, M., et al. (2018). Tearing, Segmentation, and Backstepping of Subduction in the Aegean: New Insights from Seismicity. *Tectonophysics* 734-735, 96–118. doi:10.1016/j.tecto.2018.04.002

Caputo, R., Catalano, S., Monaco, C., Romagnoli, G., Tortorici, G., and Tortorici, L. (2010). Active Faulting on the Island of Crete (Greece). *Geophys. J. Int.* 183, 111–126. doi:10.1111/j.1365-246X.2010.04749.x

Cortés-Aranda, J., González, G., Rémy, D., and Martinod, J. (2015). Normal Upper Plate Fault Reactivation in Northern Chile and the Subduction Earthquake Cycle: From Geological Observations and Static Coulomb Failure Stress (CFS) Change. *Tectonophysics* 639, 118–131. doi:10.1016/j.tecto.2014.11.019

Dolan, J. F., Bowman, D. D., and Sammis, C. G. (2007). Long-range and Long-Term Fault Interactions in Southern California. *Geol* 35, 855–858. doi:10.1130/G23789A.1

Doutsos, T., and Kokkalas, S. (2001). Stress and Deformation Patterns in the Aegean Region. *J. Struct. Geology.* 23, 455–472. doi:10.1016/S0191-8141(00)00119-X

Farías, M., Comte, D., Roecker, S., Carrizo, D., and Pardo, M. (2011). Crustal Extensional Faulting Triggered by the 2010 Chilean Earthquake: The Pichilemu Seismic Sequence. *Tectonics* 30, a–n. doi:10.1029/2011TC002888

Flemming, N. C. (1978). Holocene Eustatic Changes and Coastal Tectonics in the Northeast Mediterranean: Implications for Models of Crustal Consumption. *Phil. Trans. R. Soc. Lond. A.* 289, 405–458. doi:10.1098/rsta.1978.0065

Gaki-Papanastassiou, K., Maroukian, H., and Kourmpanian, V. (2011). The Morphotectonic Evolution of Southern Half of Kythira Island (Ionian Sea, Greece) during the Quaternary. *Pr. Geogr.* 127, 49–60.

Goodall, H. J., Gregory, L. C., Wedmore, L. N. J., Mccaffrey, K. J. W., Amey, R. M. J., Roberts, G. P., et al. (2021). Determining Histories of Slip on Normal Faults with Bedrock Scarps Using Cosmogenic Nuclide Exposure Data. *Tectonics* 40, e2020TC006457. doi:10.1029/2020TC006457

Heidbach, O., Rajabi, M., Reiter, K., and Ziegler, M.WSM Team (2016). World Stress Map Database Release 2016. V. 1.1. *GFZ Data Serv.* doi:10.5880/WSM.2016.001

Howell, A., Jackson, J., Copley, A., McKenzie, D., and Nissen, E. (2017). Subduction and Vertical Coastal Motions in the Eastern Mediterranean. *Geophys. J. Int.* 211, 593–620. doi:10.1093/gji/ggx307

Jackson, J. A., Gagnepain, J., Houseman, G., King, G. C. P., Papadimitriou, P., Soufleris, C., et al. (1982). Seismicity, normal Faulting, and the Geomorphological Development of the Gulf of Corinth (Greece): the Corinth Earthquakes of February and March 1981. *Earth Planet. Sci. Lett.* 57, 377–397. doi:10.1016/0012-821x(82)90158-3

Kato, A., Sakai, S. i., and Obara, K. (2011). A normal-faulting Seismic Sequence Triggered by the 2011 off the Pacific Coast of Tohoku Earthquake: Wholesale Stress Regime Changes in the Upper Plate. *Earth Planet. Sp* 63, 745–748. doi:10.5047/eps.2011.06.014

Kelsey, H. M., Hull, A. G., Cashman, S. M., Berryman, K. R., Cashman, P. H., Trexler, J. H., et al. (1998). Paleoseismology of an Active Reverse Fault in a Forearc Setting: The Poukawa Fault Zone, Hikurangi Forearc, New Zealand. *Geol. Soc. America Bull.* 110 (9), 1123–1148. doi:10.1130/0016-7606(1998)110<1123:poaarf>2.3.co;2

Kokinou, E., and Kamberis, E. (2009). The Structure of the Kythira-Antikythira Strait, Offshore SW Greece (35.7°-36.6°N). *Geol. Soc. Lond. Spec. Publications* 311, 343–360. doi:10.1144/SP311.14

Kokinou, E., Tiago, A., and Evangelos, K. (2012). Structural Decoupling in a Convergent Forearc Setting (Southern Crete, Eastern Mediterranean). *Geol. Soc. America Bull.* 124, 1352–1364. doi:10.1130/B30492.1

Konstantinou, K. I. (2010). Crustal Rheology of the Santorini-Amorgos Zone: Implications for the Nucleation Depth and Rupture Extent of the 9 July 1956 Amorgos Earthquake, Southern Aegean. *J. Geodynamics* 50, 400–409. doi:10.1016/j.jog.2010.05.002

Konstantinou, K. I., Kalogeras, I. S., Melis, N. S., Kourouzidis, M. C., and Stavrakakis, G. N. (2006). The 8 January 2006 Earthquake (Mw 6.7) Offshore Kythira Island, Southern Greece: Seismological, strong-motion, and Macroseismic Observations of an Intermediate-Depth Event. *Seismological Res. Lett.* 77, 544–553. doi:10.1785/gssrl.77.5.544

Konstantinou, K. I., Mouslopoulou, V., Liang, W. T., Heidbach, O., Oncken, O., and Suppe, J. (2017). Present-day Crustal Stress Field in Greece Inferred from Regional-scale Damped Inversion of Earthquake Focal Mechanisms. *J. Geophys. Res. Solid Earth* 122, 506–523. doi:10.1002/2016JB013272

Le Pichon, X., Lallemant, S. J., Chamot-Rooke, N., Lemeur, D., and Pascal, G. (2002). The Mediterranean Ridge Backstop and the Hellenic Nappes. *Mar. Geology.* 186, 111–125. doi:10.1016/S0025-3227(02)00175-5

Lekkas, E., Papanikolaou, I., Papanikolaou, D., and Danamos, G. (2008). "Correlating the Damage and the Geological structureLocal Site Effects from the 2006 Mw=6.7 Kythira Island Intermediate Depth Event, SW Greece," In Proceedings of the 14th World Conference on Earthquake Engineering, Beijing, China, October 12–17, 2008, 1–4.

Lisiecki, L. E., and Raymo, M. E. (2005). A Pliocene-Pleistocene Stack of 57 Globally Distributed Benthic δ18O Records. *Paleoceanography* 20, a–n. doi:10.1029/2004PA001071

Lyberis, N., Angelier, J., Barrier, E., and Lallemant, S. (1982). Active Deformation of a Segment of Arc: the Strait of Kythira, Hellenic Arc, Greece. *J. Struct. Geology.* 4, 299–311. doi:10.1016/0191-8141(82)90016-5

Manzocchi, T., Walsh, J. J., and Nicol, A. (2006). Displacement Accumulation from Earthquakes on Isolated normal Faults. *J. Struct. Geology.* 28, 1685–1693. doi:10.1016/j.jsg.2006.06.006

Marrett, R., and Allmendinger, R. W. (1990). Kinematic Analysis of Fault-Slip Data. *J. Struct. Geology.* 12, 973–986. doi:10.1016/0191-8141(90)90093-E

Marsellos, A. E., and Kidd, W. S. F. (2008). Extension and Exhumation of the Hellenic Forearc ridge in Kythera. *J. Geology.* 116, 640–651. doi:10.1086/591995

McClusky, S., Balassanian, S., Barka, A., Demir, C., Ergintav, S., Georgiev, I., et al. (2000). Global Positioning System Constraints on Plate Kinematics and Dynamics in the Eastern Mediterranean and Caucasus. *J. Geophys. Res.* 105, 5695–5719. doi:10.1029/1999JB900351

Mechernich, S., Schneiderwind, S., Mason, J., Papanikolaou, I. D., Deligiannakis, G., Pallikarakis, A., et al. (2018). The Seismic History of the Pisia Fault (Eastern Corinth Rift, Greece) from Fault Plane Weathering Features and Cosmogenic 36 Cl Dating. *J. Geophys. Res. Solid Earth* 123, 4266–4284. doi:10.1029/2017JB014600

Menant, A., Angiboust, S., Gerya, T., Lacassin, R., Simoes, M., and Grandin, R. (2020). Transient Stripping of Subducting Slabs Controls Periodic Forearc Uplift. *Nat. Commun.* 11, 1823. doi:10.1038/s41467-020-15580-7

Meulenkamp, J. E. (1985). "Aspects of the Late Cenozoic Evolution of the Aegean Region," in *Chp 15, Geological Evolution of the Mediterranean Basin*. Editors D. J. Stanley and F. C. Wezel (New York: Springer-Verlag). doi:10.1007/978-1-4613-8572-1_15

Meulenkamp, J. E., Theodoropoulos, P., and Tsapralis, V. (1977). Remarks on the Neogene of Kythira, Greece. *Sixth Coll. Geol. Aegean Region* 1, 355–362.

Moore, G. F., Boston, B. B., Sacks, A. F., and Saffer, D. M. (2013). Analysis of normal Fault Populations in the Kumano Forearc Basin, Nankai Trough, Japan: 1. Multiple Orientations and Generations of Faults from 3-D Coherency Mapping. *Geochem. Geophys. Geosyst.* 14 (6), 1989–2002. doi:10.1002/ggge.20119

Mountjoy, J. J., and Barnes, P. M. (2011). Active Upper Plate Thrust Faulting in Regions of Low Plate Interface Coupling, Repeated Slow Slip Events, and Coastal Uplift: Example from the Hikurangi Margin, New Zealand. *Geochem. Geophys. Geosystems* 12 (1). doi:10.1029/2010gc003326

Mouslopoulou, V., Begg, J., Nicol, A., Oncken, O., and Prior, C. (2015b). Formation of Late Quaternary Paleoshorelines in Crete, Eastern Mediterranean. *Earth Planet. Sci. Lett.* 431, 294–307. doi:10.1016/j.epsl.2015.09.007

Mouslopoulou, V., Bocchini, G. M., Cesca, S., Saltogianni, V., Bedford, J., Petersen, G., et al. (2020). Earthquake Swarms, Slow Slip and Fault Interactions at the Western-End of the Hellenic Subduction System Precede the M W 6.9 Zakynthos Earthquake, Greece. *Geochem. Geophys. Geosyst.* 21, e2020GC009243. doi:10.1029/2020GC009243

Mouslopoulou, V., Moraetis, D., Benedetti, L., Guillou, V., Bellier, O., and Hristopulos, D. (2014). Normal Faulting in the Forearc of the Hellenic Subduction Margin: Paleoearthquake History and Kinematics of the Spili Fault, Crete, Greece. *J. Struct. Geology.* 66, 298–308. doi:10.1016/j.jsg.2014.05.017

Mouslopoulou, V., Nicol, A., Begg, J., Oncken, O., and Moreno, M. (2015a). Clusters of Megaearthquakes on Upper Plate Faults Control the Eastern Mediterranean hazard. *Geophys. Res. Lett.* 42, 10282–10289. doi:10.1002/2015GL066371

Mouslopoulou, V., Nicol, A., Walsh, J. J., Begg, J. G., Townsend, D. B., and Hristopulos, D. T. (2012). Fault-slip Accumulation in an Active Rift over Thousands to Millions of Years and the Importance of Paleoearthquake Sampling. *J. Struct. Geology.* 36, 71–80. doi:10.1016/j.jsg.2011.11.010

Mouslopoulou, V., Saltogianni, V., Nicol, A., Oncken, O., Begg, J., Babeyko, A., et al. (2019). Breaking a Subduction-Termination from Top to Bottom: The Large 2016 Kaikōura Earthquake, New Zealand. *Earth Planet. Sci. Lett.* 506, 221–230. doi:10.1016/j.epsl.2018.10.020

Mouslopoulou, V., Walsh, J. J., and Nicol, A. (2009). Fault Displacement Rates on a Range of Timescales. *Earth Planet. Sci. Lett.* 278, 186–197. doi:10.1016/j.epsl.2008.11.031

Mozafari, N., Tikhomirov, D., Sumer, Ö., Özkaymak, Ç., Uzel, B., Yeşilyurt, S., et al. (2019). Dating of Active normal Fault Scarps in the Büyük Menderes Graben (Western Anatolia) and its Implications for Seismic History. *Quat. Sci. Rev.* 220, 111–123. doi:10.1016/j.quascirev.2019.07.002

Nicol, A., Mouslopoulou, V., Begg, J., and Oncken, O. (2020a). Displacement Accumulation and Sampling of Paleoearthquakes on Active Normal Faults of Crete in the Eastern Mediterranean. *Geochem. Geophys. Geosyst.* 21, e2020GC009265. doi:10.1029/2020GC009265

Nicol, A., Van Dissen, R. J., Stirling, M. W., and Gerstenberger, M. C. (2016). Completeness of the Paleoseismic Active-Fault Record in New Zealand. *Seismological Res. Lett.* 87, 1299–1310. doi:10.1785/0220160088

Nicol, A., Walsh, J., Berryman, K., and Villamor, P. (2006). Interdependence of Fault Displacement Rates and Paleoearthquakes in an Active Rift. *Geol* 34, 865–868. doi:10.1130/G22335.1

Nicol, A., Walsh, J., Childs, C., and Manzocchi, T. (2020b). "The Growth of Faults," in *Chapter 6 in Understanding Faults: Detecting, Dating, and Modelling*. Editors D. Tanner and C. Brandes (Amsterdam: Elsevier), 221–255. doi:10.1016/B978-0-12-815985-9.00006-0

Nicol, A., Walsh, J. J., Villamor, P., Seebeck, H., and Berryman, K. R. (2010). Normal Fault Interactions, Paleoearthquakes and Growth in an Active Rift. *J. Struct. Geology.* 32, 1101–1113. doi:10.1016/j.jsg.2010.06.018

Nicol, A., Walsh, J., Mouslopoulou, V., and Villamor, P. (2009). Earthquake Histories and Holocene Acceleration of Fault Displacement Rates. *Geology* 37, 911–914. doi:10.1130/G25765A.1

Nicol‡, A., Walsh, J. J., Watterson, J., and Underhill, J. R. (1997). Displacement Rates of normal Faults. *Nature* 390, 157–159. doi:10.1038/36548

Papadopoulos, G. A., and Vassilopoulou, A. (2001). "Historical and Archaeological Evidence of Earthquakes and Tsunamis Felt in the Kythira Strait, Greece," in *Tsunami Research at the End of a Critical Decade*. Editor G. T. Hebenstreit (Dordrecht: Springer), 119–138. doi:10.1007/978-94-017-3618-3_10

Papanikolaou, D., and Danamos, G. (1991). The Geotectonic Position of Kythera and Cyclades within the Geodynamic Evolution of the Hellenic Arc. *Bull. Geol. Soc. Greece* XXV, 65–74.

Papanikolaou, D. J., and Royden, L. H. (2007). Disruption of the Hellenic Arc: Late Miocene Extensional Detachment Faults and Steep Pliocene-Quaternary normal Faults-Or what Happened at Corinth? *Tectonics* 26, a–n. doi:10.1029/2006TC002007

Papazachos, B. C., and Papazachou, K. (1997). *The Earthquakes of Greece*. Thessaloniki: Ziti editions.

Petit, J. P. (1987). Criteria for the Sense of Movement on Fault Surfaces in Brittle Rocks. *J. Struct. Geology.* 9, 597–608. doi:10.1016/0191-8141(87)90145-3

Petrocheilos, J. (1966). Geological Map of Kythera Island. Institute for Geology and Subsurface Research, Athens. Scale 1, 50,000.

Pirazzoli, P. A., Thommeret, J., Thommeret, Y., Laborel, J., and Montag-Gioni, L. F. (1982). Crustal Block Movements from Holocene Shorelines: Crete and Antikythira (Greece). *Tectonophysics* 86, 27–43. doi:10.1016/0040-1951(82)90060-9

Rabineau, M., Berné, S., Olivet, J.-L., Aslanian, D., Guillocheau, F., and Joseph, P. (2006). Paleo Sea Levels Reconsidered from Direct Observation of Paleoshoreline Position during Glacial Maxima (For the Last 500,000 Yr). *Earth Planet. Sci. Lett.* 252, 119–137. doi:10.1016/j.epsl.2006.09.033

Robertson, J., Meschis, M., Roberts, G. P., Ganas, A., and Gheorghiu, D. M. (2019). Temporally Constant Quaternary Uplift Rates and Their Relationship with

Extensional Upper-Plate Faults in South Crete (Greece), Constrained With36Cl Cosmogenic Exposure Dating. *Tectonics* 38, 1189–1222. doi:10.1029/2018TC005410

Sadler, P. M. (1981). Sediment Accumulation Rates and the Completeness of Stratigraphic Sections. *J. Geology.* 89, 569–584. doi:10.1086/628623

Sakellariou, D., and Tsampouraki-Kraounaki, K. (2019). "Plio-Quaternary Extension and Strike-Slip Tectonics in the Aegean," in *Transform Plate Boundaries and Fracture Zones*. Editor J. C. Duarte (Amsterdam: Elsevier), 339–374. doi:10.1016/b978-0-12-812064-4.00014-1

Saltogianni, V., Mouslopoulou, V., Oncken, O., Nicol, A., Gianniou, M., and Mertikas, S. (2020). Elastic Fault Interactions and Earthquake Rupture along the Southern Hellenic Subduction Plate Interface Zone in Greece. *Geophys. Res. Lett.* 47, e2019GL086604. doi:10.1029/2019GL086604

Sasvári, Á., and Baharev, A. (2014). SG2PS (Structural Geology to Postscript Converter) - A Graphical Solution for Brittle Structural Data Evaluation and Paleostress Calculation. *Comput. Geosciences* 66, 81–93. doi:10.1016/j.cageo.2013.12.010

Schurr, B., Asch, G., Hainzl, S., Bedford, J., Hoechner, A., Palo, M., et al. (2014). Gradual Unlocking of Plate Boundary Controlled Initiation of the 2014 Iquique Earthquake. *Nature* 512, 299–302. doi:10.1038/nature13681

Shaw, B., Ambraseys, N. N., England, P. C., Floyd, M. A., Gorman, G. J., Higham, T. F. G., et al. (2008). Eastern Mediterranean Tectonics and Tsunami hazard Inferred from the AD 365 Earthquake. *Nat. Geosci* 1, 268–276. doi:10.1038/ngeo151

Shaw, B., and Jackson, J. (2010). Earthquake Mechanisms and Active Tectonics of the Hellenic Subduction Zone. *Geophys. J. Int.* 181, 966–984. doi:10.1111/j.1365-246X.2010.04551.x

Shirzaei, M., Bürgmann, R., Oncken, O., Walter, T. R., Victor, P., and Ewiak, O. (2012). Response of Forearc Crustal Faults to the Megathrust Earthquake Cycle: InSAR Evidence from Mejillones Peninsula, Northern Chile. *Earth Planet. Sci. Lett.* 333-334, 157–164. doi:10.1016/j.epsl.2012.04.001

Tesson, J., Pace, B., Benedetti, L., Visini, F., Delli Rocioli, M., Arnold, M., et al. (2016). Seismic Slip History of the Pizzalto Fault (central Apennines, Italy) Using In Situ-produced36Cl Cosmic ray Exposure Dating and Rare Earth Element Concentrations. *J. Geophys. Res. Solid Earth* 121, 1983–2003. doi:10.1002/2015JB012565

Tiberti, M. M., Basili, R., and Vannoli, P. (2014). Ups and downs in Western Crete (Hellenic Subduction Zone). *Sci. Rep.* 4, 5677–7. doi:10.1038/srep05677

Townsend, D., Nicol, A., Mouslopoulou, V., Begg, J., Beetham, R., Clark, D., et al. (2010). Palaeoearthquake Histories across a normal Fault System in the Southwest Taranaki Peninsula, New Zealand. *New Zealand J. Geology. Geophys.* 53, 375–394. doi:10.1080/00288306.2010.526547

van Hinsbergen, D. J. J., Hafkenscheid, E., Spakman, W., Meulenkamp, J. E., and Wortel, R. (2005). Nappe Stacking Resulting from Subduction of Oceanic and continental Lithosphere below Greece. *Geol* 33, 325–328. doi:10.1130/G20878.1

van Hinsbergen, D. J. J., Van der Meer, D. G., Zachariasse, W. J., and Meulenkamp, J. E. (2006). Deformation of Western Greece during Neogene Clockwise Rotation and Collision with Apulia. *Int. J. Earth Sci. (Geol Rundsch)* 95, 463–490. doi:10.1007/s00531-005-0047-5

Veliz, V., Mouslopoulou, V., Nicol, A., Fassoulas, C., Begg, J., and Oncken, O. (2018). Millennial to Million Year normal-fault Interactions in the Forearc of a Subduction Margin, Crete, Greece. *J. Struct. Geology.* 113, 225–241. doi:10.1016/j.jsg.2018.05.019

Vilanova, S. P., Nunes, C. F., and Fonseca, J. F. (2003). Lisbon 1755: A Case of Triggered Onshore Rupture? *Bull. Seismological Soc. America* 93, 2056–2068. doi:10.1785/0120020245

Wallace, R. E. (1977). Profiles and Ages of Young Fault Scarps, north-central Nevada. *Geol. Soc. America Bull.* 88, 1267–1281. doi:10.1130/0016-7606(1977)88<1267:paaoyf>2.0.co;2

Walsh, J. J., Childs, C., Manzocchi, T., Imber, J., Nicol, A., Meyer, V., et al. (2001). "Geometrical Controls on the Evolution of Normal Fault Systems," in *The Nature of the Tectonic Significance of Fault Zone Weakening*. Editors R. E. Holdsworth (London: Geological Society) Special Publications, 186, 157–170.

Walsh, J. J., and Watterson, J. (1991). "Geometric and Kinematic Coherence and Scale Effects in normal Fault Systems," in *The Geometry of Normal Faults*. *Geological Society, London, Special Publications*. Editors A. M. Roberts, G. Yielding, and B. Freeman, 56, 193–203. doi:10.1144/GSL.SP.1991.056.01.13

Wang, T., Wei, S., Shi, X., Qiu, Q., Li, L., Peng, D., et al. (2018). The 2016 Kaikōura Earthquake: Simultaneous Rupture of the Subduction Interface and Overlying Faults. *Earth Planet. Sci. Lett.* 482, 44–51. doi:10.1016/j.epsl.2017.10.056

Wells, D. L., and Coppersmith, K. J. (1994). New Empirical Relationships Among Magnitude, Rupture Length, Rupture Width, Rupture Area, and Surface Displacement. *Bull. Geol. Soc. Am.* 84, 974–1002.

Wesnousky, S. G. (2008). Displacement and Geometrical Characteristics of Earthquake Surface Ruptures: Issues and Implications for Seismic-hazard Analysis and the Process of Earthquake Rupture. *Bull. Seismological Soc. America* 98, 1609–1632. doi:10.1785/0120070111

Zhang, H., He, Z., Ma, B., Long, J., Liang, K., and Wang, J. (2017). The Vertical Slip Rate of the Sertengshan piedmont Fault, Inner Mongolia, China. *J. Asian Earth Sci.* 143, 95–108. doi:10.1016/j.jseaes.2017.04.014

**Conflict of Interest:** The authors declare that the research was conducted in the absence of any commercial or financial relationships that could be construed as a potential conflict of interest.